Eccentric contraction during gait is associated with muscle fat replacement in Duchenne Muscular Dystrophy

by Ruben Boon
student number 4241371
Delft University of Technology

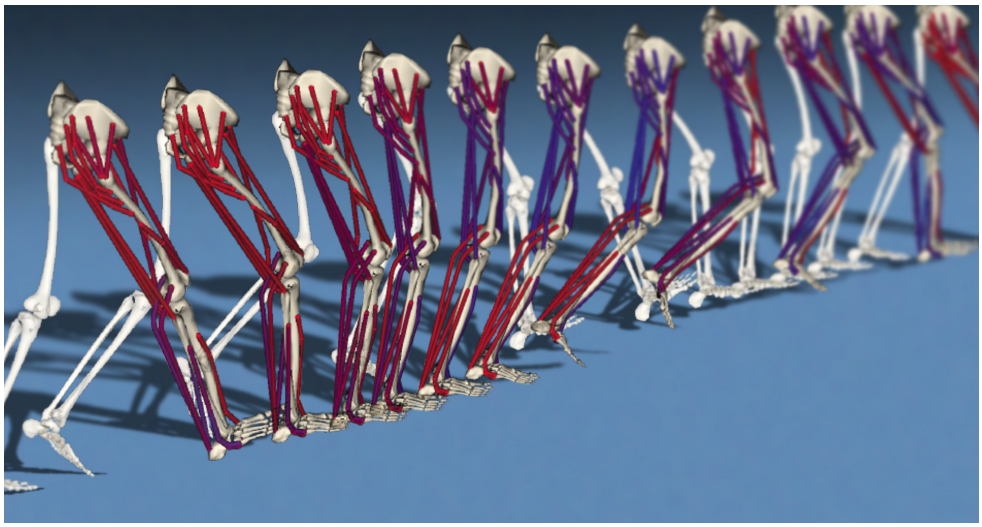

Thesis Submitted in Partial Fulfillment of the Requirements
for the Degree of Master of Science

Department of Biomedical Engineering
Faculty of 3mE

Supervisors:
Prof. dr. ir. J. Harlaar
Dr. ir. J.H. De Groot
A. Seth
T.T.J. Veeger
K. Veerkamp

Contents

1 Introduction

1.1 Background

1.1.1 Duchenne Muscular Dystrophy

Duchenne muscular dystrophy (DMD) is an x-linked recessive neuromuscular disorder affecting 1 in 3,500-5,000 new-born males [1]. DMD is caused by absence of functional dystrophin, a protein expressed in muscle [2], and is characterized by progressive muscle weakness, where muscles show progressive damage and degeneration [3]. First symptoms due to muscle weakness become apparent before the age of 6 [4]. As muscle weakness progresses, DMD patients lose the ability to walk independently and become bound to a wheelchair in their early teens [1]. Death usually occurs in the third or fourth decade of their lives resulting from cardiorespiratory impairment [1].

Muscles of DMD patients become increasingly susceptible to damage over time and undergo several structural and compositional changes, including inflammation, edema and fiber necrosis. Ultimately, muscle tissue is irreversibly replaced with fibrous tissue and fatty deposit, which can be visualized with magnetic resonance imaging (MRI) [5, 6]. Interestingly, muscles of DMD patients are not equally affected since differences in muscle fat fractions, which quantify the ratio between healthy, contractile muscle and fat replacement, are evident [7–9], as illustrated in Figure 1.

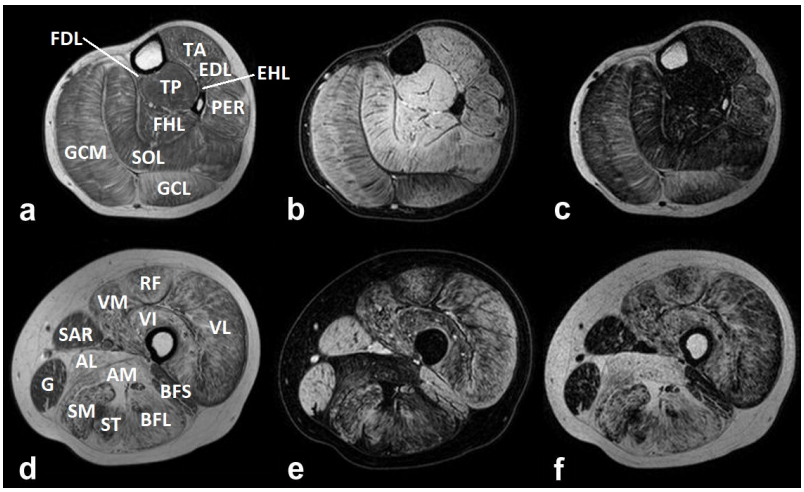

Figure 1: Different signal intensities are evident from a T1-weighted and Dixon MR image of the upper and lower right leg. T1-weighted (a,d), Dixon water (b,e) and Dixon fat (c,f) image of upper and lower leg muscles of an eleven year old DMD patient. **Upper leg muscles**: rectus femoris (RF), vastus lateralis (VL), vastus intermedius (VI), vastus medialis (VM), sartorius (SAR), adductor longus (AL), adductor magnus (AM), gracilis (G), semimembranosus (SM), semitendinosus (ST), biceps femoris long head (BFL) and biceps femoris short head (BFS). **Lower leg muscles**: tibialis anterior (TA), tibialis posterior (TP), flexor digitorum longus (FDL), extensor digitor longus (EDL), flexor hallucis longus (FHL), extensor hallucis longus (EHL), peroneus (PER), soleus (SOL), gastrocnemius medialis (GCM) and gastrocnemius lateralis (GCL). Adapted from Wokke et al. (2014) [10].

Despite a large amount of literature on the responsible gene and its product, dystrophin, the process leading from absence of functional dystrophin to muscle degeneration, and ultimately fat replacement, is still not well understood [3, 11]. To this date, several hypotheses coexist, such as mechanical and signaling deficits and impaired calcium homeostasis in muscle tissue [11]. Remaining ambulant as long as possible is important for DMD patients, since remaining functionally independent and socially engaged increases the quality of their lives [12]. Besides, sedentary behavior is known to accelerate the process of muscle atrophy and induces other health risks like increased fat mass, diabetes, heart disease and more [13]. The question remains to what extent muscle use is beneficial for preservation of muscle tissue in DMD patients [14]. Aerobic exercise interventions showed delayed functional decline in some muscular dystrophies, including DMD [13]. On the other hand, adverse effects of exercise include muscle damage due to structural fragility or signaling deficits [3]. As such, understanding of a possible mechanical role in muscle degeneration, and ultimately fat replacement, may result in strategies to prolong muscle function.

Therefore, the aim of this study is to explain differences in fat replacement among muscles of DMD patients by mechanical factors. Musculoskeletal simulation provides a method to estimate individual muscle contributions during daily activities that are otherwise unable to acquire [15]. In the next section, an overview of studies describing muscle fat replacement in DMD is presented, after which background information regarding a role of dystrophin-absence in muscle damage and force loss is presented. Next, a preliminary study that used musculoskeletal simulation to predict muscle fat replacement is discussed [16]. The introduction is concluded with a study design to investigate a possible mechanical role in explaining differential muscle fat replacement in DMD.

1.1.2 Muscle fat replacement

Muscle fat replacement is associated with disease progression and correlates with functional outcome measures like peak force production [17–19]. Muscle fat fraction, the ratio between healthy, contractile muscle and muscle fat replacement, can be quantified with MRI (qMRI). The accumulation of muscle fat replacement is age-dependent and follows an 'S-shaped' curve [20, 21]. Individual leg muscles are affected at different stages and with variable progressions, but ultimately result in a more or less consistent successive pattern of fat replacement [17].

Fat fractions of individual leg muscles of a population of 16 DMD patients can be ordered from highest to lowest fat fraction, as illustrated in Figure 2. An order starting with the adductor magnus, followed by the quadriceps and hamstrings muscles and relative sparing of the sartorius and gracilis muscles can be observed in the upper leg. Lower leg muscles are generally affected later, which is in line with a proximal-to-distal gradient in the progression of muscle weakness [10].

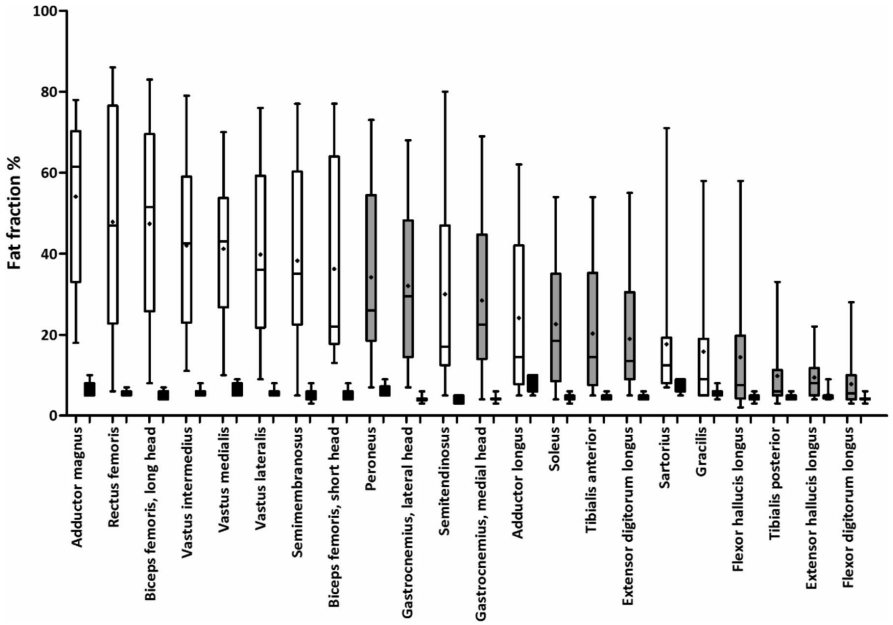

Figure 2: Box-and-Whisker plot of the fat fractions per muscle in the upper and lower leg of DMD patients (n = 16, age = 11.4 ± 2.2) and healthy controls (n = 11, age = 10.7 ± 2.1). Fat fractions are shown for DMD patients in the upper leg (white) and lower leg (grey) and for healthy controls (black). Values shown as median (-) and mean (·) ± interquartile range and standard deviation. The muscles are ordered by mean values [10].

In order to summarize the order of fat fractions derived from different studies, a color-scale of the order of individual leg muscles was created to show similarities between studies, listed in Table 1. In the first 7 studies qMRI was used to acquire fat fractions. Other studies used semi- or non-quantitative evaluation. In these studies, MR images were scored with the Mercuri scale (semi-qMRI) [9], or were visually scored (non-qMRI). To quantify robustness of the positions of muscles in the order fat fractions, the positions in the order were numbered for each study separately, after which the root mean square error (RMSE) of the position was calculated for each muscle as follows:

$$RMSE=\sqrt{\sum w(P_i - O_i)^2 / \sum w} \tag{1}$$

where P_i represents the predicted position based on minimizing the sum of all RMSE values, O_i the observed position and w the weight of the error. It was chosen that $w = 3$ for qMRI, $w = 2$ for semi-qMRI and $w = 1$ for non-qMRI. The resulting summary of the orders of fat fractions among studies is shown in Figure 3, in which the muscles are ranked based on predicted position ($P_{Gmax} = 1$). If the FF or position of the $Gmax$ was not reported in a study, the predicted position of the AM shifted to 1, et cetera. The numbers of the studies in the first column of the table correspond to the first column numbers in the figure.

Table 1: Authors, number of participants, number of analyzed muscles, field strength and scoring technique for each included DMD study.

	authors	participants	muscles	B field	scoring
1	Akima et al. (2010) [17]	n=28	12	1,5/3T	qMRI
2	Barnard et al. (2018) [19]	n=136	8	3T	qMRI
3	Gaeta et al. (2012) [7]	n=22	8	1,5T	qMRI
4	Mankodi et al. (2016) [22]	n=13	6	3T	qMRI
5	Ponrartana et al. (2015) [23]	n=13	16	3T	qMRI
6	Wokke et al. (2014) [10]	n=16	18	3T	qMRI
7	Yin et al. (2019) [8]	n=32	11	3T	qMRI
8	Godi et al. (2012) [24]	n=26	20	3T	semi-qMRI
9	Polavarapu et al. (2016) [25]	n=50	19	1,5T	semi-qMRI
10	Kim et al. (2010) [26]	n=34	13	1,5T	semi-qMRI
11	Li et al. (2015) [27]	n=170	13	1,5/3T	semi-qMRI
12	Marden et al. (2005) [28]	n=10	8	1,5T	non-qMRI

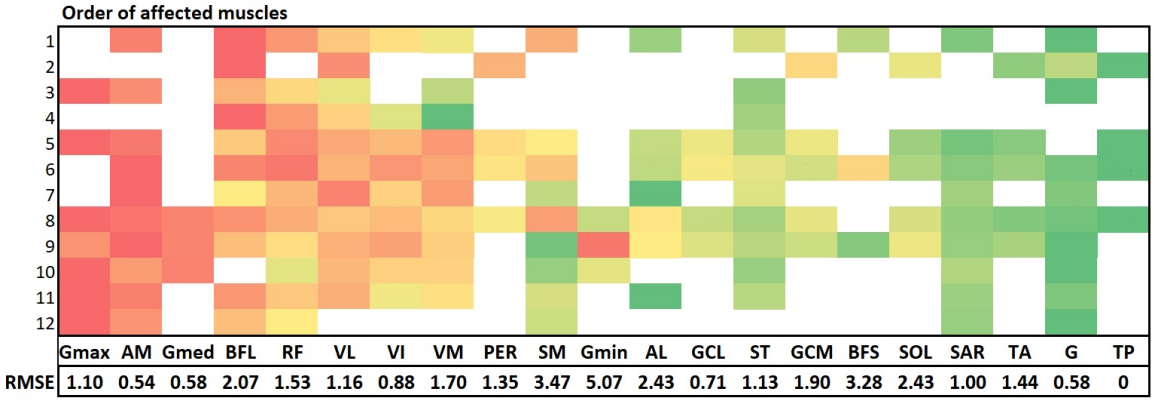

Figure 3: Color-scales representing the order of muscle fat fractions from twelve different studies, in which the ranks of the muscles are based on minimizing the sum of RMSE values. The row numbers correspond to the studies and details listed in Table 1. Included muscles: gluteus maximus (Gmax), adductor magnus (AM), gluteus medius (Gmed), biceps femoris, long head (BFL), rectus femoris (RF), vastus lateralis (VL), vastus intermedius (VI), vastus medialis (VM), peroneus (PER), semimembranosus (SM), gluteus minimus (Gmin), adductor longus (AL), gastrocnemius lateralis (GCL), semitendinosus (ST), gastrocnemius medialis (GCM), biceps femoris short head (BFS), soleus (SOL), sartorius (SAR), tibialis anterior (TA), gracilis (G) and tibialis posterior (TP).

From Figure 3, it can be seen that the order of muscle fat fractions in DMD patients is generally agreeable between studies. Early involvement of the gluteus maximus (Gmax), adductor magnus (AM) and gluteus medius (Gmed) is obvious from all studies, as well as relative sparing of the sartorius (SAR), gracilis (G), tibialis anterior (TA) and tibialis posterior (TP). Positions of some of the other muscles differ somewhat between studies. Higher RMSE values, found in the gluteus minimus (Gmin), semimembranosus (SM) and biceps femoris, short head (BFS), indicate insecurity regarding the position in the order.

1.1.3 Dystrophin-absence and muscle damage

Dystrophin connects cytoskeletal γ actin to extracullar matrix via a group of proteins in the surface membrane, the dystrophin-associated glycoprotein complex (DGC), as illustrated in Figure 4 [2, 29]. Together with additional cytoskeletal proteins, the DGC forms rib-like lattices on the sarcolemma called costameres [30]. Costameres act as mechanical couplers to distribute contractile forces generated in the sarcomere laterally through the sarcolemma [31]. Based on its structure and location, it is suggested that the main function of the DGC is to mechanically stabilize the sarcolemma during muscle contraction [11].

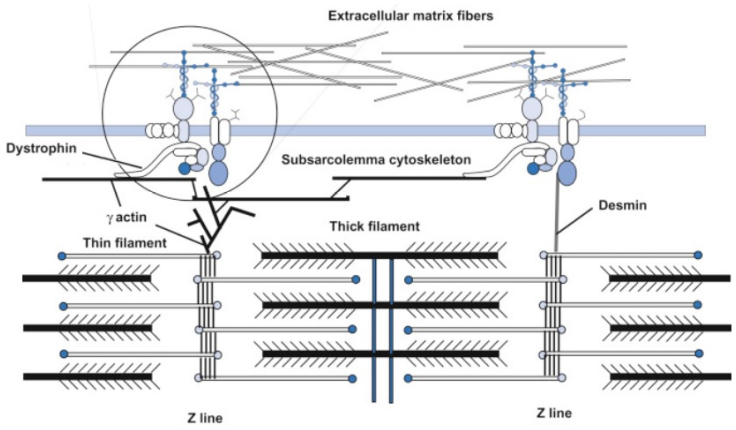

Figure 4: The dystrophin associated glycoprotein complex (DGC) consists of cytosolic proteins, transmembrane proteins, and extracellular proteins that link the myofilaments to the extracellular matrix through cytoskeleton filaments. In the DGC, Z-lines are linked to dystrophin through γ actin cytoskeletal filaments. Adapted from Feher (2017) [32].

Absence of dystrophin causes the DGC to be functionally impaired, making the sarcolemma more susceptible to damage when subjected to mechanical stress. Breaches in the sarcolemma cause inhomogeneous sarcomere activation due to leaking calcium channels [11]. Combined with a lack of lateral force transmission [31], this leads to concentrated forces on the remaining longitudinal pathway of muscle fibers [33]. During eccentric contraction, the muscle-tendon complex lengthens while contracting, thereby absorbing energy generated by external loads [34]. This type of contraction is especially harmful for dystrophin-absent muscle in *mdx* mice, a commonly used animal model for DMD [35, 36], since the eccentric loading is to be absorbed predominantly by the contractile proteins and titin, which acts as a molecular spring in muscle [33, 37].

Peak force production is decreased in *mdx* muscle and is further decreased after eccentric contraction induced muscle damage [38]. The work done to lengthen muscle fibers is strongly related to the magnitude of damage in *mdx* muscle [39]. Dystrophin is normally abundant at the myotendinous junction, the interface between muscle and tendon, as well as at the neuromuscular junction, the area of synaptic contact between muscle and nerve [40]. Dystrophin-absence at the myotendinous junction may result in fiber detachment and thus decreased force transmission between muscle and

bone [33], while dystrophin-absence at the neuromuscular junction may result in structural abnormalities that impair excitation-contraction (EC) coupling [41]. Fiber branching, in which a fiber splits, such that it composes of multiple continuous strands, may also play a role in decreased peak force in *mdx* muscle, since asynchronous contraction causes extra stress on the branch points [42]. Interestingly, malformed fibers are especially found in longer *mdx* muscle fibers, which seem to be more susceptible to damage [43].

In humans, eccentric contraction is also associated with muscle damage [44, 45]. Furthermore, structural abnormalities resulting from eccentric contraction induced muscle damage are thought to also occur in DMD, since it was found that the time delay between the onset of fascicle motion and force production is progressively increased in the biceps brachii of DMD patients [46, 47].

1.1.4 Simulation of DMD muscle loading

Hu and Blemker (2015) used 3-dimensional musculoskeletal simulation (OpenSim) to test for a relation between muscle fat replacement and normalized negative work of 22 muscles during one gait cycle. Normalized negative work was calculated by taking the time-integral of normalized negative power, such that:

$$W_{neg,norm} = \int \frac{F \cdot v_{neg}}{F_{max} \cdot L} \tag{1}$$

where F represents the active force, F_{max} the maximal isometric force, v_{neg} the lengthening velocity (i.e., eccentric contraction) and L the instantaneous fiber length of the muscle [16]. Similarly, positive work was calculated by replacing v_{neg} with v_{pos} to quantify concentric contraction. Normalization of work was done to account for variations in fiber length and differences in physiological cross-sectional area (PCSA), which is strongly associated to force production [48]. Gait analysis was chosen because walking is one of the most common daily activities, albeit not an activity that generates the largest amount of negative work in muscles [16].

Linear regression between fat percentages and negative work values were performed for the upper and lower leg separately, as illustrated in Figure 5. Negative work was highly correlated to fat fractions, only except for the adductor magnus and peroneus, two hallmark muscles that show the highest fat fractions in the upper and lower leg, respectively. Excluding these two muscles yielded significant relations in both the upper and lower leg muscles, suggesting an association between eccentric contraction and different progressions of muscle fat replacement in DMD [16].

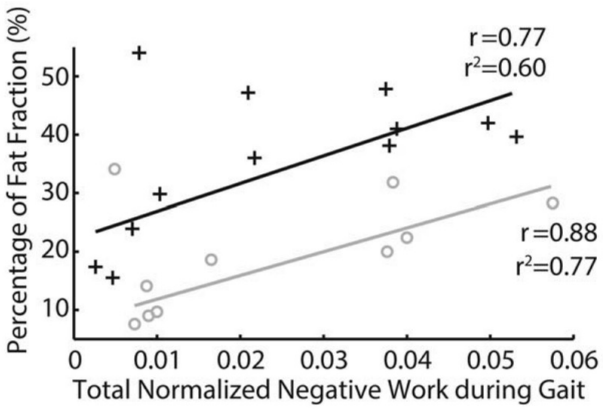

Figure 5: Negative work was highly correlated with fat fraction for both upper and lower leg muscles separately, except for the adductor magnus in the upper leg and the peroneus in the lower leg. Copied from Hu and Blemker (2015) [16].

A limitation of this study is that the used model was based on an unimpaired adult man walking at self-selected speed [49, 50], while DMD patients never develop a typical, mature gait pattern [51–54]. Furthermore, negative work values were normalized to PCSA and fiber length. Both fiber length as well as the interaction of PCSA and fiber length are associated with muscle fat replacement in DMD [55]. Therefore, analyzing the individual effects of negative work, PCSA and fiber length on fat replacement may yield additional insight regarding a mechanical role in explaining differential fat replacement among leg muscles of DMD patients.

1.2 Study design

1.2.1 Simulating gait in children

Musculoskeletal simulation is widely used to predict kinematics, dynamics and energy consumption of gait and improve the functional performance during rehabilitation, to increase sports performance or discover strategies to prevent injuries [15, 49, 56]. By prediction, musculoskeletal modelling allows insight into physiological mechanisms involved with movement that are otherwise unable to be measured, such as joint loading, neural control and detailed individual muscle contributions [15].

In the study presented in section 1.1.4, Hu and Blemker (2015) analyzed one gait cycle, illustrated in Figure 6, of an unimpaired adult man walking at self-selected speed [16]. Gait kinematics (joint angles) of children are similar to those of adults by 3,5-4 years of age [57]. However, kinetics (internal joint moments) differ from adults until at least 7 years of age [58]. Before reaching adult-like kinematics during gait, children especially show decreased plantarflexion moments in the ankle [59]. It is suggested that children lack neuromuscular maturity to produce ankle power patterns similar to those of adults until 9 years of age [57, 59], and rely more on hip power during stance [60]. As gait in children has matured, kinematic and kinetic differences with adult gait, as well as differences in EMG patterns, can mainly be attributed to differences in normalized walking speed [61, 62].

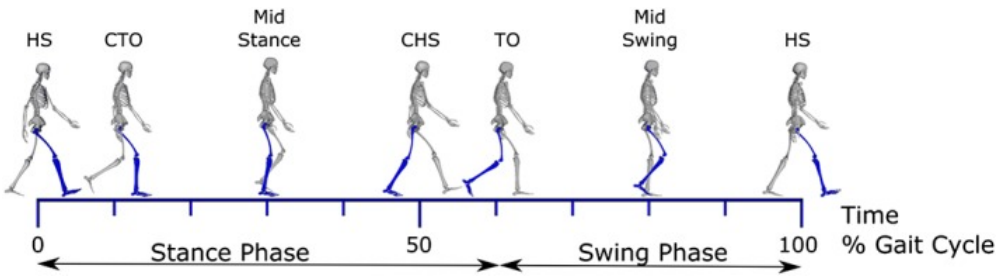

Figure 6: The gait cycle, beginning and ending with right heel strike. The stance phase, in which the right leg has contact with the ground, accounts for 62% of the gait cycle. The remaining 38% accounts for swing phase, in which the right leg is off the ground. HS = heel strike; CTO = contralateral toe off the ground; CHS = contralateral heel strike; TO = toe off. Copied from Cheung et al. (2016) [63]

In this study, gait simulation was applied to compute muscle contributions in multiple gait cycles of a small cross-sectional sample of unimpaired children. This way, differences between participants as well as differences within participant was compensated for. Furthermore, the eccentric loading, i.e. negative work, resulting from the simulations was used to predict differences in muscle degeneration, quantified by the order of muscle fat replacement among individual muscles. In order to do so, the method of the study performed by Hu and Blemker (2015) [16] was applied to gait of multiple children, after which an extension of their analysis was performed. Furthermore, in the extended analysis, negative work was not normalized to fiber length and PCSA, such that muscle architecture and total negative work are separated into two independent variables that both predict the dependent variable, muscle fat replacement.

1.2.2 Research question

The following research question was formulated:

Is eccentric contraction during gait associated with muscle fat replacement in individual leg muscles of Duchenne Muscular Dystrophy patients?

In order to answer this research question, the following goals were defined. The first goal was to apply the method of Hu and Blemker to gait of children [16]. Specifically, for each gait cycle, normalized negative and positive work was calculated for each individual muscle in one leg. Furthermore, linear regressions between normalized negative and positive work and fat fraction values were computed for upper and lower leg muscles separately. Upper and lower leg muscles were separated in this analysis to explain why upper leg muscles generally show higher fat fractions than lower leg muscles, while normalized negative work values were similar. If the findings of Hu and Blemker (2015) are generally true, similar or better trends should be found in children.

The second goal was to extend the analysis by (1) evaluating effects of leg part of the muscle (upper or lower) on fat replacement and (2) to analyze individual effects of muscle architecture and total negative work on muscle fat replacement. If upper leg muscles are more strongly associated to muscle fat replacement than lower leg muscles, we should see a significant effect of the interaction between leg part and normalized negative work on muscle fat replacement. Furthermore, if muscle

architecture is an independent factor associated to muscle fat replacement, a strong effect should be found in a multiple regression model, which also applies for the other independent factor, total negative work. It was hypothesized that both eccentric contraction as well as muscle architecture are associated to muscle fat replacement in DMD. Furthermore, it was hypothesized that normalized negative work during gait in upper leg muscles is not more strongly associated to fat replacement than in lower leg muscles. In the next section, the study method is outlined.

2 Materials and method

2.1 Materials

2.1.1 Subjects

Five unimpaired children were included for this study. No girls were included because only males are affected by DMD. The five youngest subjects were selected from a group of fifteen (age 8.8 ± 2.5) because their kinematics during gait should differ most with respect to adults [58]. The onset of symptoms due to muscle weakness in DMD is earlier than the ages of the included subjects. Therefore, gait patterns of younger children are thought to be more similar to those of DMD patients than older children or adults. More specifications of the included subjects are listed in Table 2 below, where we normalized walking speed according to an equation proposed by Hof et al. (1996) [64]:

$$v^* = \frac{v}{\sqrt{g \cdot L_{leg}}} \tag{2}$$

where v^* represents normalized walking speed, v walking speed, g the gravitational acceleration constant and L_{leg} the leg length.

Table 2: Specifications of the included subjects.

Specifications	Mean (standard deviation)
Gender	Male: 5
Age (years)	7.16 (0.994)
Weight (kg)	23.5 (4.08)
Height (cm)	1.25 (0.0785)
Normalized walking speed	0.529 (0.0612)

The sole inclusion criterion for the subjects was that they should not have any neurological or neuromuscular problems. All measurements were performed at the Clinical Motion Analysis Laboratory of the University Hospital of Pellenberg (CMAL-Pellenberg) [65, 66].

2.1.2 Data collection

Gait kinematics, kinetics and muscle activities were collected as participants walked barefoot over a 10 meter level walkway at self-selected walking speed. A set of 15 markers with 14-millimeter diameter of the lower limb Plug-in-Gait (PiG) model was used and markers were tracked with a 10 to 15-camera VICON system (Nexus 1.8.4. Vicon-UK, Oxford, UK) at a sample frequency of 100 Hz. Ground reaction forces were collected with two force plates embedded in the walkway (AMTI, Watertown, MA, USA). Muscle activities of the gluteus maximus, rectus femoris, vastus lateralis, medial hamstrings, medial gastrocnemius, soleus and tibialis anterior were recorded with surface electromyography (sEMG) bilaterally with a 16-channel telemetric system (Zerowire, Cometa, Italy) at 1000 or 1500 Hz. The sEMG electrodes were attached according to SENIAM recommendations

[65, 66].

Muscle fat fractions of 16 DMD patients (age 11.4 ± 2.2) reported by Wokke et al. (2014) were used for this study. Another set of muscle fat fractions was pulled from the LUMC database to append to the dataset presented by Wokke et al. (2014), such that a more complete set of fat fractions was generated. The appended set of fat fractions were pulled from 16 DMD patients (age 10.1 ± 2.6) and included the rectus femoris (RF), vastus lateralis (VL), vastus intermedius (VI), vastus medialis (VM), biceps femoris long head (BFL), biceps femoris short head (BFS), semitendinosus (ST), semimembranosus (SM), adductor magnus (AM), adductor longus (AL), gracilis (GR) and sartorius (SAR) in the upper leg. Fat fractions of lower leg muscles included the gastrocnemius lateralis (GCL), gastrocnemius medialis (GCM), soleus (SOL), tibialis anterior (TA), tibialis posterior (TP), extensor digitorum longus (EDL) and peroneus (PER). The fat fraction of the gluteus maximus (Gmax) was calculated with the z-score, which was acquired by taking fat fractions of 15 muscles acquired by Ponrartana et al. (2015) [23], such that:

$$Z_{Gmax}=\frac{Gmax_{FF}-\mu_{FF}}{\sigma_{FF}} \tag{3a}$$

where $Gmax_{FF}$ is the fat fraction of the gluteus maximus, μ_{FF} the mean fat fraction of all included muscles except $Gmax$ and σ_{FF} the standard deviation of the fat fractions of all included muscles except $Gmax$. The z-score of the $Gmax$ was then used to calculate the mean fat fraction of the $Gmax$ in the dataset used in this study, such that:

$$Gmax_{FF}=\mu_{FF} + Z_{Gmax} \cdot \sigma_{FF} \tag{3b}$$

Fat fractions of the extensor hallucis longus (EHL), flexor digitorum longus (FDL), flexor hallucis longus (FHL) were calculated similarly, using fat fractions reported by Wokke et al. (2014) [10]. Mean fat fractions and standard deviations of upper and lower leg muscles of the total group of 32 DMD patients (age 10.8 ± 2.4) are illustrated in Figure 7 below.

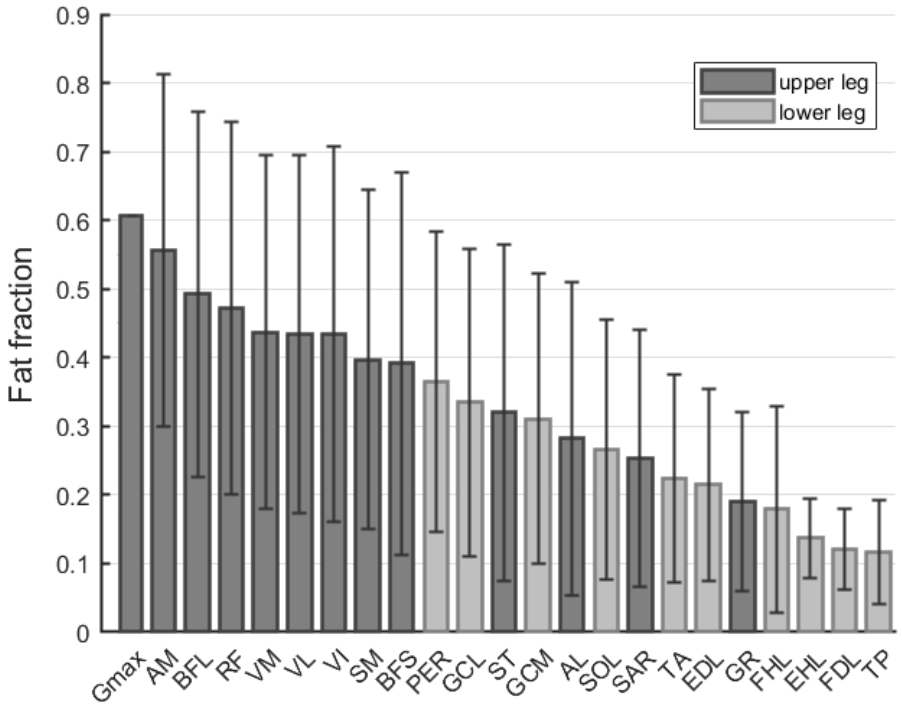

Figure 7: Fat fractions (means and standard deviations) of upper and lower leg muscles: gluteus maximus (Gmax), adductor magnus (AM), biceps femoris long head (BFL), rectus femoris (RF), vastus medialis (VM), vastus lateralis (VL), vastus intermedius (VI), semimembranosus (SM), biceps femoris short head (BFS), peroneus (PER), gastrocnemius lateralis (GCL), semitendinosus (ST), gastrocnemius medialis (GCM), adductor longus (AL), soleus (SOL), sartorius (SAR), tibialis anterior (TA), extensor digitorum longus (EDL), gracilis (GR), flexor hallucis longus (FHL), extensor hallucis longus (EHL), flexor digitorum longus (FDL) and tibialis posterior (TP).

The order of fat fractions (FF) from Figure 7 is highly agreeable to the order presented in Figure 3, in which the FF order was summarized from twelve studies. A difference is that the position of the biceps femoris short head (BFS) is several ranks higher than predicted. As mentioned, the BFS has a high RMSE, indicating insecurity regarding its position in the FF order. Also, the gastrocnemii (GCL and GCM) and semitendinosus (ST) have higher FFs than the adductor longus (AL), in contrast to the predicted order. The ranks of these four muscles were more or less interchangeable in the position of the FF order without having a large effect on the sum of the RMSE values. Lastly, the extensor digitorum longus (EDL), extensor hallucis longus (EHL), flexor digitorum longus (FDL) and flexor hallucis longus (FHL) were not included in Figure 3 since only one of the twelve studies reported FF values of these muscles [10].

Muscle architecture parameters PCSA and optimal fiber length (L_f) were extracted from Ward et al. (2009) [67]. The reported PCSA values took pennation angle of the muscles into account in order to relate PCSA to force, such that:

$$PCSA = \frac{mass[g] \cdot \cos(\theta)}{fiber\ \ length[cm] \cdot \rho[\frac{g}{cm^3}]} \quad (4)$$

where θ represents the pennation angle (degrees). In this study, "classical" PCSA values were used, representing cross-sectional areas perpendicular to the muscle fibers. Therefore, the reported PCSA values were divided by the cosine of the pennation angles as reported in the same study.

2.1.3 Data processing

Kinematic and kinetic data were extracted from C3D files, the standard file format in motion capture, and filtered with a 6 Hz second order low-pass Butterworth filter. Virtual markers in the pelvis were added to the original kinematic files, such that the pelvis could be scaled in three dimensions. EMG data were filtered with a recursive, second order Butterworth bandpass filter between 30 and 300 Hz before rectification and filtering with a 6 Hz second order low-pass Butterworth filter. EMGs were normalized to the highest signal value found for each muscle during the trial. Subsequently, a time delay of 40 milliseconds was added to the EMGs to correct for electromechanical delay between surface EMG signal and force production [68]. For each participant, at least three representative gait cycles from initial contact to initial contact, containing accurate foot placement on the embedded force plates, were selected for further analysis.

2.2 Method

2.2.1 Musculoskeletal simulation

A scaled model of each participant was created using OpenSim (version 4.1) [15]. The gait2392 model [50], a generic model containing 23 degrees of freedom and 92 musculotendon units, representing 76 muscles in the lower extremities and torso, was used. Fiber lengths and PCSA values of the gait2392 model were extracted from Wickiewicz et al. (1983) [69] or Friederich et al. (1990) [70] and scaled to approach muscle parameters of a 26 year-old instead of an elderly cadaver. Using the scaling tool in OpenSim, body segments, musculotendon units and its parameters were linearly scaled by matching the model's virtual markers to the participant's experimental markers during a static pose. Body mass was scaled proportionally over the body segments to maintain mass distribution. Virtual markers at joint centers are calculated by software associated with the PiG model by VICON. Maximal marker errors were minimized by increasing the weight of markers at bony landmarks. The resulting static pose of the model is illustrated in Figure 8 and was verified by checking associated videos of the participants.

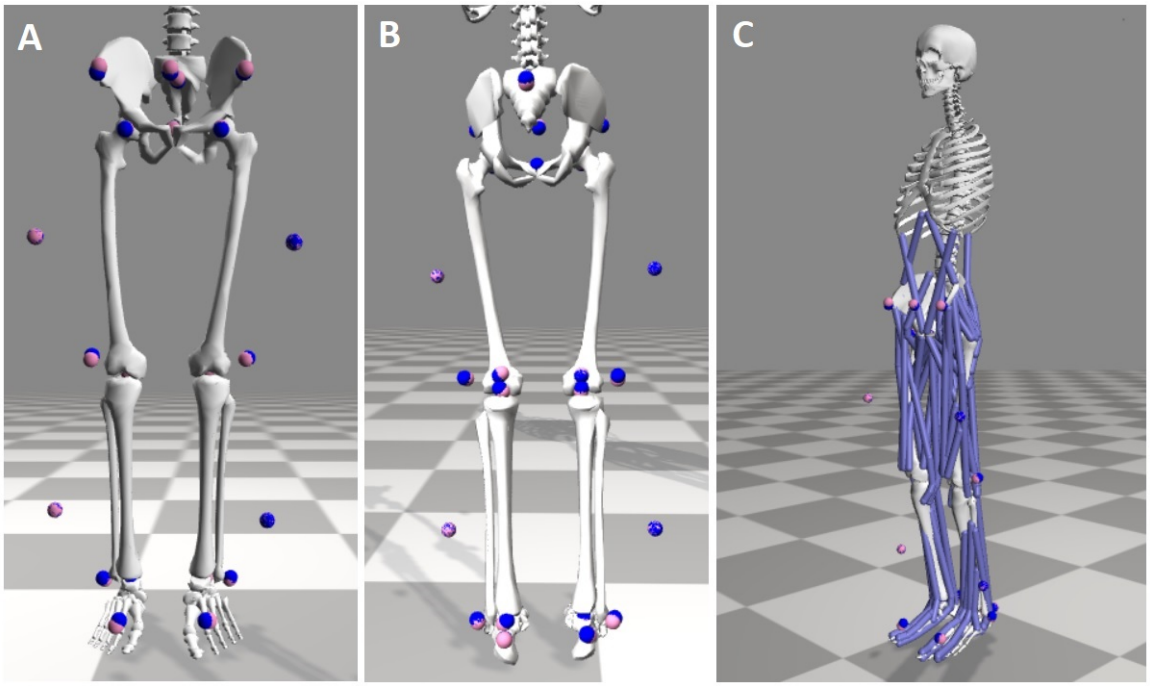

Figure 8: Front view (**A**), rear view (**B**) and static pose (**C**) of a scaled model showing errors between virtual model markers (pink) and experimental markers (blue). Musculotendon units were hidden in **A** and **B** to expose markers.

When maximal marker errors of below 10 millimeters were achieved, the inverse kinematics tool was used to track marker positions during gait. It was evaluated if the scaled model also showed low maximal marker errors during gait. In most cases, maximal RMSE values of below 10 millimeters was achieved (18/20 analyzed gait cycles), half of which showed maximal marker errors of below 10 millimeters (9/20 analyzed gait cycles), indicating an anatomically accurate model of the participant. The maximal isometric force (MIF) of the musculotendon units were subsequently scaled according to the following formula [71]:

$$MIF_{new}=MIF_{model}\cdot\left(\frac{mass_{new}}{mass_{model}}\right)^{\frac{2}{3}} \tag{5}$$

Joint angles resulting from inverse kinematics were visually compared to existing literature of typically developing children [61], after which the inverse dynamics tool was used to calculate joint moments, using inverse kinematics and associated ground reaction forces as input. Ground reaction forces (GRFs) as well as hip abduction/adduction, hip flexion/extension, knee flexion/extension and ankle dorsiflexion/plantarflexion moments were normalized by body mass and compared to existing literature as well [61]. Figure 9 shows joint angles resulting from inverse kinematics of one gait cycle and Figure 10 shows the corresponding joint angle moments resulting from inverse dynamics. A more detailed comparison to reference literature is found in Appendix A.

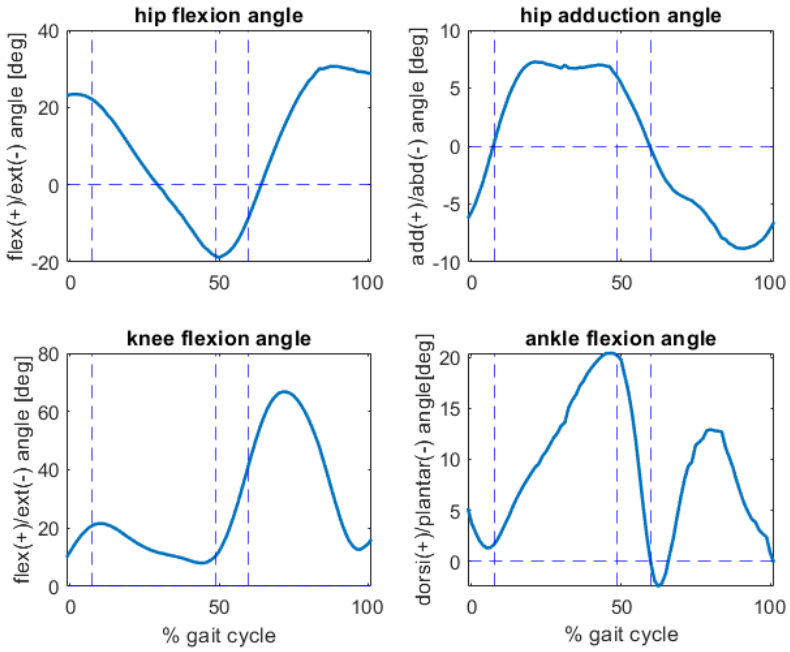

Figure 9: Joint angles resulting from inverse kinematics of one representative gait cycle.

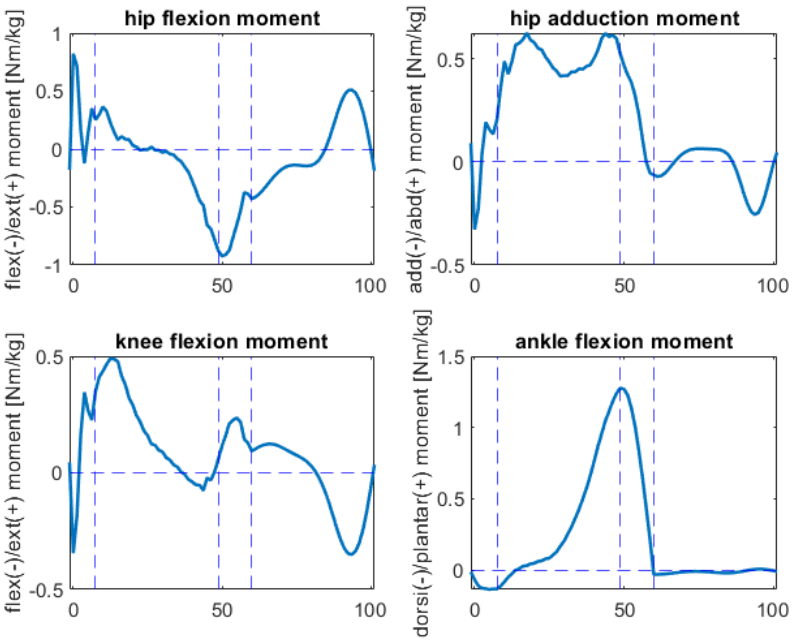

Figure 10: Joint angle moments resulting from inverse dynamics of one representative gait cycle.

After inverse dynamics, dynamic inconsistencies were reduced to allow more accurate force calculations. Dynamic inconsistencies between kinematics and GRFs can occur from marker data processing errors and are associated with lower simulation quality. The residual reduction algorithm (RRA) tool alters torso mass center of the model and allows for small kinematic deviations to reduce dynamic inconsistencies.

To calculate muscle forces and activations, the static optimization (SO) or computed muscle control (CMC) tool can be used. SO resolves joint angle moments resulting from inverse dynamics into individual muscle forces at each time instant by minimizing the sum of the squared muscle activations. The CMC tool is an extension of SO, in which muscle excitations that drive the simulation to a desired kinematic trajectory are predicted. Specifically, muscle excitations resulting in specific joint angles, joint angular velocities and associated muscle states (activations and lengths) are computed using a combination of proportional-derivative (PD) control and SO (Figure 11). Since accurate muscle states were needed to compute muscle power, the CMC tool was best suited for this study.

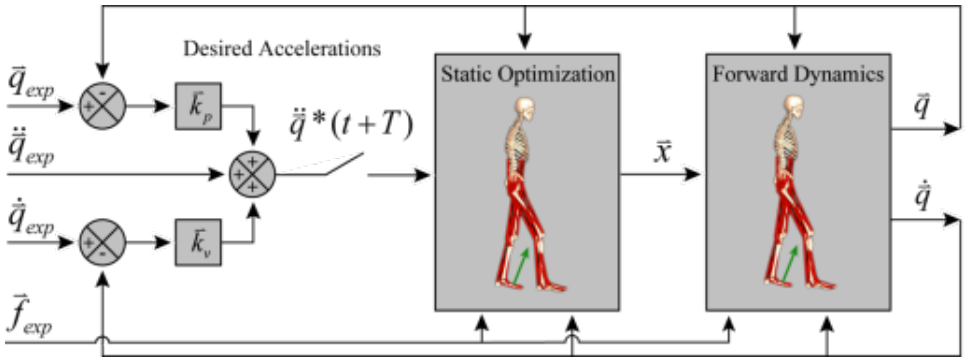

Figure 11: Schematic of the Computed Muscle Control algorithm applied to gait simulation [72].

2.2.2 Computed muscle control analysis

Muscle activations resulting from CMC simulations were compared to associated EMG signals, which were also compared to EMGs from existing literature [61, 68]. Oftentimes, muscles showed activation peaks at initial heel contact and toe off. These peaks may be related to a lack of accurate modeling of short range stiffness (SRS) in muscles, which is the relatively high stiffness muscles exhibit just after length change over a short time interval [73]. Underestimation of the SRS could cause the musculotendon unit to overestimate the activation needed to generate the force needed to absorb external loading. The activation peaks are probably also associated with spikes in hip and knee flexion moment resulting from remaining dynamic inconsistency. Especially muscles associated with these types of moments, like the gastrocnemius and hamstrings muscles for knee flexion and the rectus femoris for hip flexion, showed such activation peaks. To overcome this, these muscles were constrained from excitation in parts of the gait cycles where EMGs did not show activation, as illustrated in Figure 12. Constraining muscles affects power, and thus negative and positive work, as illustrated in Figure 13.

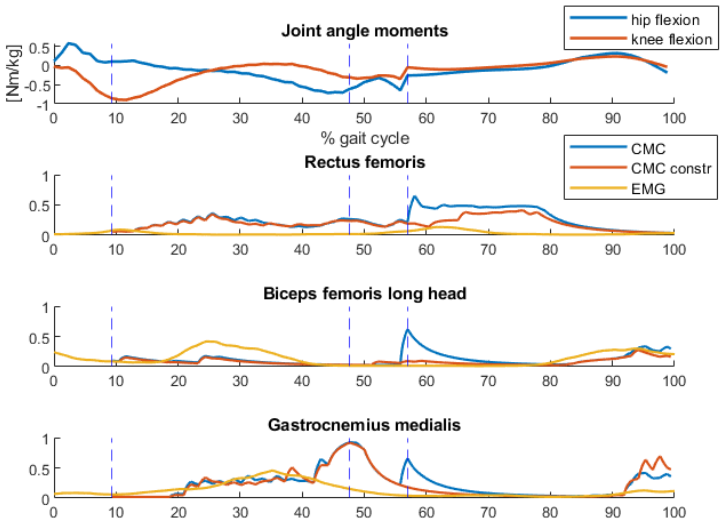

Figure 12: Spikes in hip and knee flexion moment during toe off cause activation peaks in several muscles. Constraining them (CMC constr) results in higher agreement with EMG. The striped vertical lines indicate gait cycle events, from left to right: contralateral toe off (CTO), contralateral heel strike (CHS) and toe off (TO).

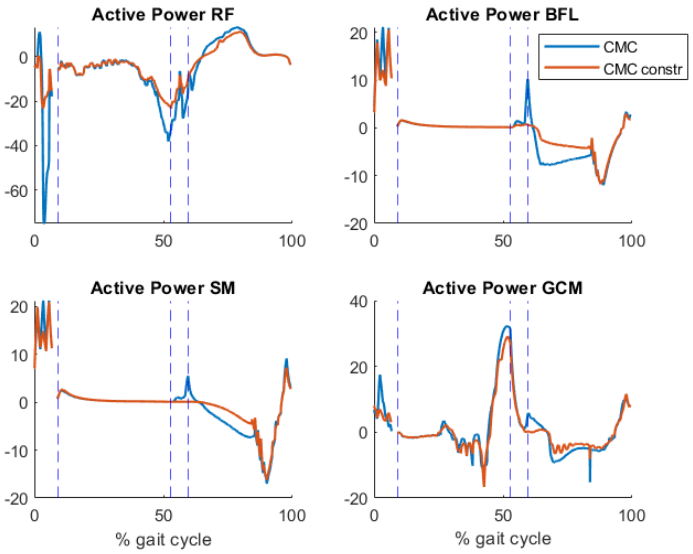

Figure 13: Constraining (CMC constr) the rectus femoris (RF), biceps femoris long head (BFL), semimembranosus (SM) and gastrocnemius medialis (GCM) affects power and thus work. Power of the first 10% was taken from double stance of the contralateral leg. The striped vertical lines indicate gait cycle events, from left to right: contralateral toe off (CTO), contralateral heel strike (CHS) and toe off (TO).

Since only two force plates were embedded in the floor, GRFs of the contralateral foot were missing during the first double stance phase, as illustrated in Figure 14. Since this causes the CMC tool to fail, muscle states of the first part of each gait cycle were missing, accounting for approximately 10%. Therefore, the muscle force and states of the contralateral leg during double stance, approximately between 50-60% of the gait cycle, were added to the force and states of the main analyzed leg. Further analysis was performed with Matlab (The Mathworks Inc., Natick, M.A., 2020a).

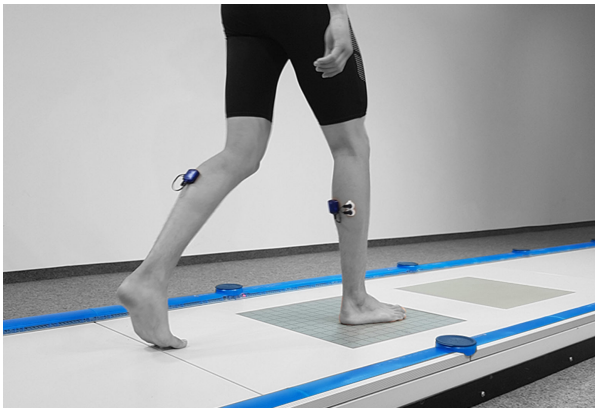

Figure 14: GRFs of one foot were missing during the first part of each gait cycle. Taken from https://contemplas.com/en/motion-analysis/gait-analysis/.

2.2.3 Data analysis

Similarities between muscle activations from CMC and EMGs were quantified with the normalized cross-correlation function [74]:

$$R = \frac{\sum x_i y_i}{(\sum x_i^2)^{\frac{1}{2}} (\sum y_i^2)^{\frac{1}{2}}} \tag{6}$$

where x_i represents the normalized value of the EMG signal between 0 and 1 and y_i the normalized value of the muscle activation between 0 and 1. When timing and shape of the two signals correspond well, higher values of R are found. Generally, if $R = 0.70$ or higher, the correlation was considered strong and $0.50 < R < 0.70$ was considered moderately strong [75]. Constraining usually resulted in $R > 0.50$, except for some cases where timing between the signals was off.

Two sets of results were generated. The first set includes normalized positive and negative work, calculated in the same manner as Hu and Blemker (2015) [16]. The second set of results includes total positive and negative work, and was calculated without taking maximal isometric force and fiber length into account:

$$W_{neg,tot} = \int F \cdot v_{neg} \tag{7}$$

The two sets of results were averaged over the gait cycles of each participant, and subsequently averaged over the subjects. Standard deviations were pooled with the following formula:

$$SD_{pld} = \sqrt{\frac{(n_1-1)\cdot s_1^2+(n_2-1)\cdot s_2^2+...+(n_k-1)\cdot s_k^2}{n_1+n_2+...+n_k-k}} \tag{8}$$

where n_1 represents the number of analyzed gait cycles of subject 1, s_1 the standard deviation of a certain muscle of subject 1 and k the number of included subjects.

2.2.4 Statistics

In the first part of the results, the method of the study of Hu and Blemker (2015) [16] was applied to multiple gait cycles of multiple children. Therefore, a linear regression model was built for upper and lower leg muscles separately, where positive and negative normalized work was analyzed separately.

The second part of the results is an extension of the study of Hu and Blemker (2015) [16]. Since the accumulation of age-dependent muscle fat replacement follows an 'S-shaped' curve rather than a linear relationship [20, 21, 55], a logit transform was applied to the fat fractions in this analysis to establish a linear relationship between age and fat fractions:

$$logFF = ln(\frac{FF}{1-FF}) \tag{9}$$

This transformation also causes the predicted fat fraction values to be bounded between 0 and 1. This analysis included all leg muscles, and analyzed if the relation between normalized negative work and fat fractions differs between upper and lower leg muscles. The multiple-regression model that was built for this purpose is shown in equation 10:

$$logFF = \beta_0 + \beta_1 \cdot W_{neg,norm} + \beta_2 \cdot Part + \beta_3 \cdot W_{neg,norm} \cdot Part \tag{10}$$

where $Part$ is a tag that defines whether a muscle is found in the upper or lower leg, and $W_{neg,norm} \cdot Part$ represents an interaction term. Furthermore, a linear model was built to test for an association between $logFF$ and normalized negative work for all leg muscles simultaneously.

In the third part of the results, a multiple-regression model was built that included both muscle architecture and total negative work. First, multiple-regression between $logFF$ and muscle architecture parameters optimal fiber length (L_f) and $PCSA$ was analyzed to validate results from Veeger et al. (2021), in which a significant association between interaction term $L_f \cdot PCSA$ and fat replacement was shown [55]. A total of twenty-three muscles are analyzed in the multiple-regression analysis. To minimize the number of independent variables in the model, L_f and $PCSA$, taken from Ward et al. (2009) [67], were multiplied to acquire muscle volume (V_{mus}). The models built for this purpose are defined in equations 11 and 12:

$$logFF = \beta_0 + \beta_1 \cdot L_f + \beta_2 \cdot PCSA + \beta_3 \cdot L_f \cdot PCSA \tag{11}$$

$$logFF = \beta_0 + \beta_1 \cdot W_{neg,tot} + \beta_2 \cdot V_{mus} + \beta_3 \cdot W_{neg,tot} \cdot V_{mus} \tag{12}$$

The models and associated graphs were built using R (R Core Team, version 4.1.1) and associated libraries *ggplot2*, *plotly* and *visreg*. Multiple-R^2 and p-values were used to quantify variance and significance respectively, both of which computed in R. Significance level was set at $p < .05$.

3 Results

In the first part of this section, the method of the study of Hu and Blemker (2015) [16] was applied to multiple gait cycles of multiple children. The second part of the results was an extension of this study, in which the separate effects of normalized negative work on muscle fat replacement for upper and lower leg muscles are shown. Also, the association between normalized negative work and muscle fat replacement of all muscles was analyzed. In the third part of the results, separate effects on logFF of two individual predictors, muscle architecture and total negative work, were evaluated.

Similarities between average EMG signals and average muscle activations resulting from CMC simulation are illustrated in Figure 15.

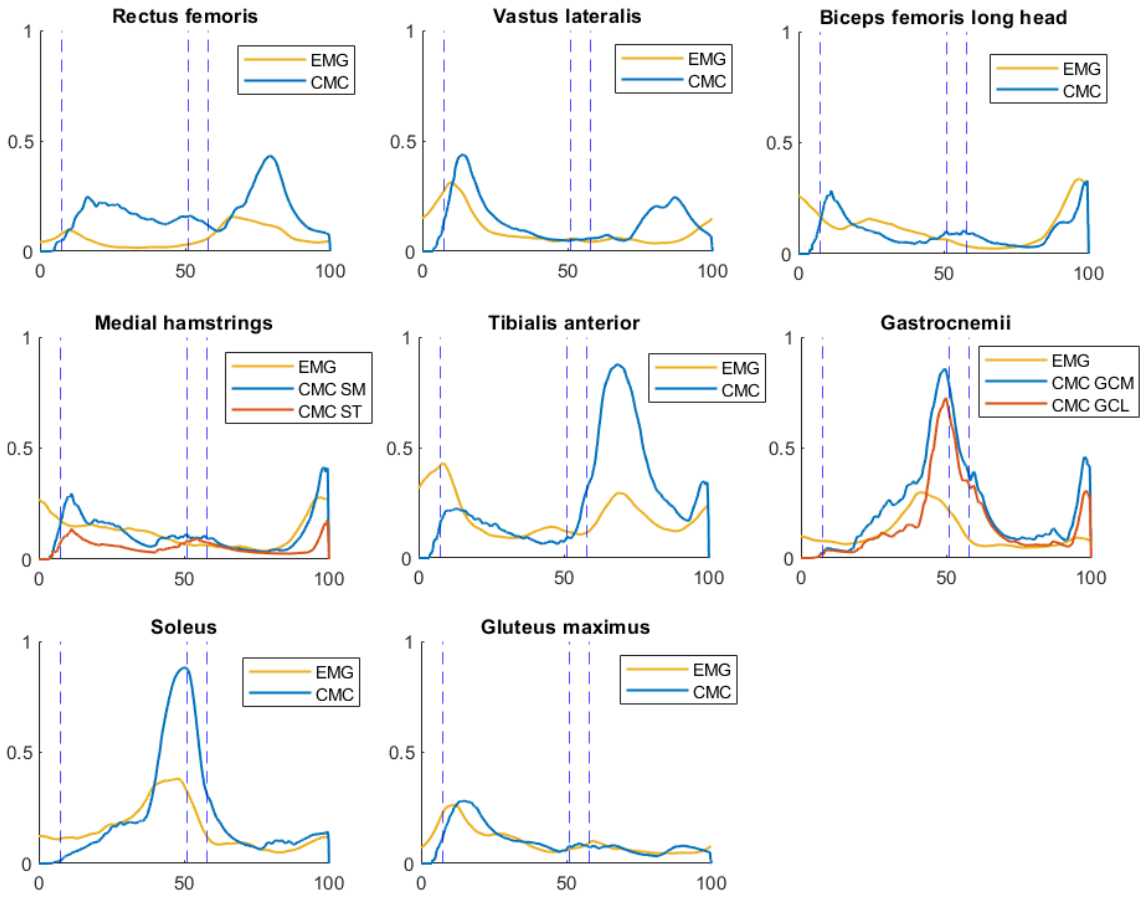

Figure 15: Similarities between average EMG signals and average muscle activations resulting from CMC simulation. The striped vertical lines indicate gait cycle events, from left to right: contralateral toe off (CTO), contralateral heel strike (CHS) and toe off (TO).

Cross-correlations between EMGs and activations resulting from CMC were computed for eight muscles to quantify similarities in timing and shape, as illustrated in Figure 16.

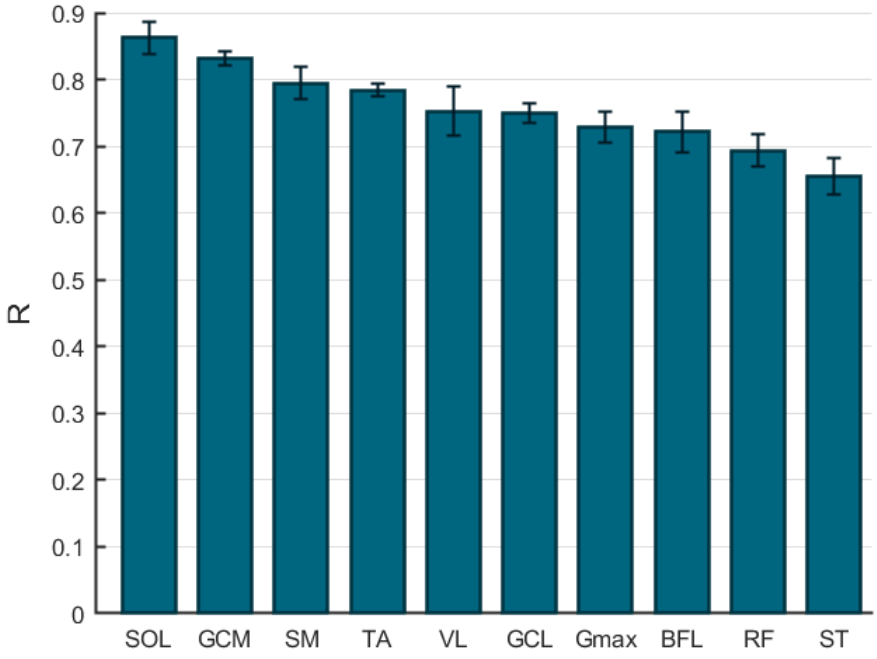

Figure 16: Cross-correlations (means & pooled standard deviations) between EMG signals and muscle activations resulting from CMC simulation, including the soleus (SOL), gastrocnemius medialis (GCM), semimembranosus (SM), tibialis anterior (TA), vastus lateralis (VL), gluteus maximus (Gmax), biceps femoris long head (BFL), rectus femoris (RF), semitendinosus (ST).

A threshold for R-values that indicate a 'strong' cross-correlation was set at 0.70 [75]. In that regard, all muscles show strong cross-correlations between EMGs and muscle activations, except for the R-values of the rectus femoris and semitendinosus, which can be considered moderately strong.

3.1 Differences with Hu and Blemker (2015)

3.1.1 Normalized negative work values

Figure 17 shows a correlation between normalized negative work values of upper leg muscles of this study and Hu and Blemker (2015). The rectus femoris (RF) and adductor magnus (AM) show the highest amounts of normalized negative work in this study, and the adductor longus (AL), semitendinosus (ST), sartorius (SAR) and gracilis (GR) show relatively low amounts of normalized negative work. The gluteus maximus (Gmax) was not included in this graph, its normalized negative work value can be found in Appendix B.

One difference between results is that the average normalized negative value of the included upper leg muscles was approximately twice as high in our study (0.050 versus an estimated 0.024).

Furthermore, the rectus femoris (RF) is the muscle with the highest normalized negative work value in this study, far exceeding the values of other muscles, while it was ranked fifth in the study of Hu and Blemker (2015). The biggest difference is the position of the adductor magnus (AM) in the order of normalized negative work values, which is ranked second in our study and ninth in the study of Hu and Blemker (2015). Apart from these two differences, the order of normalized negative work values shows a moderately strong correlation between studies for upper leg muscles ($R^2 = 0.40$, $p < .05^*$).

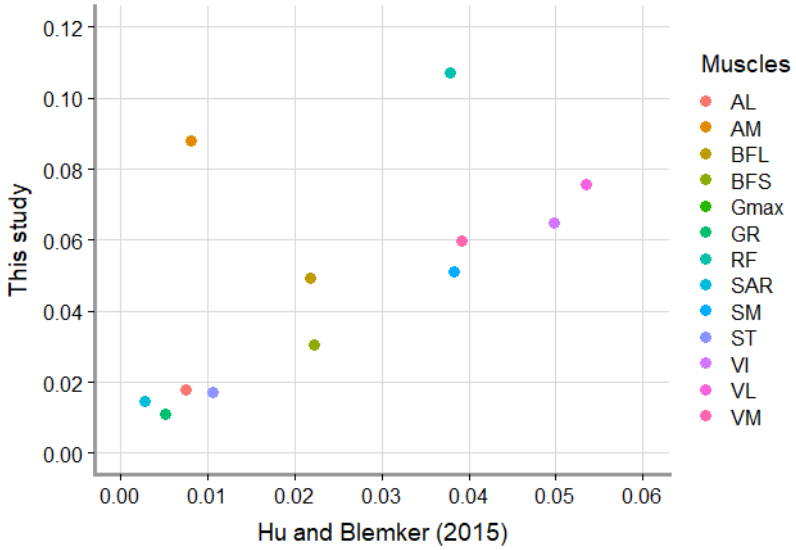

Figure 17: Correlation between normalized negative work values of upper leg muscles between this study and Hu and Blemker (2015). Included muscles: rectus femoris (RF), adductor magnus (AM), vastus lateralis (VL), vastus intermedius (VI), vastus medialis (VM), semimembranosus (SM), biceps femoris long head (BFL), biceps femoris short head (BFS), adductor longus (AL), semitendinosus (ST), sartorius (SAR), gracilis (GR).

Figure 18 shows a correlation of normalized negative work values of lower leg muscles between this study and Hu and Blemker (2015). The gastrocnemius medialis (GCM) shows the highest value and five muscles, the peroneus (PER), extensor hallucis longus (EHL), tibialis posterior (TP), flexor hallucis longus (FHL) and flexor digitorum longus (FDL) show relatively low amounts of normalized negative work.

Again, a difference between results is that the average normalized negative work values of the included lower leg muscles is approximately twice as high in this study (0.043 versus an estimated 0.023). Apart from that, the order normalized negative work values correlates very strongly between studies for lower leg muscles ($R^2 = 0.96$, $p < .001^{***}$).

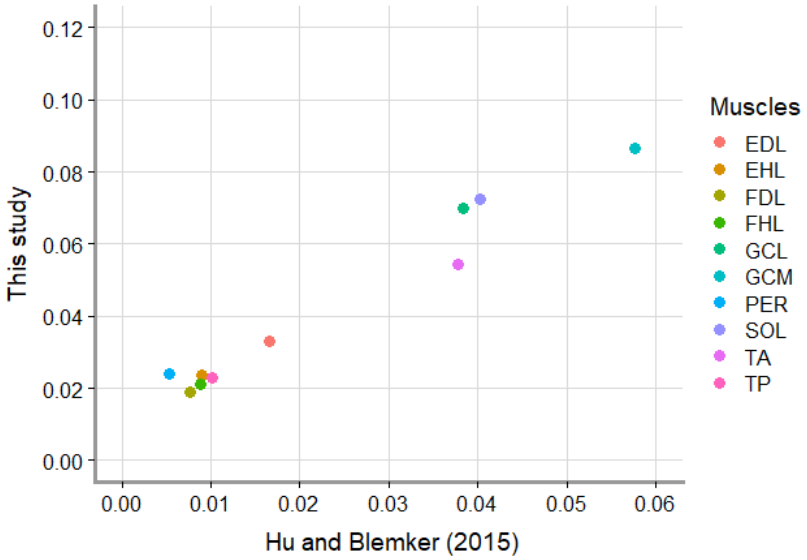

Figure 18: Correlation between normalized negative work values of lower leg muscles between this study and Hu and Blemker (2015). Included muscles: gastrocnemius medialis (GCM), soleus (SOL), gastrocnemius lateralis (GCL), tibialis anterior (TA), extensor digitorum longus (EDL), peroneus (PER), extensor hallucis longus (EHL), tibialis posterior (TP), flexor hallucis longus (FHL) and flexor digitorum longus (FDL).

3.1.2 Linear regression analysis

Linear regressions between normalized negative work and fat fractions are visualized in Figure 19A. Regressions published by Hu and Blemker (2015) are visualized in Figure 19B [16]. For upper leg muscles, normalized negative work during gait was strongly correlated to fat fractions ($R^2 = 0.63$, $p < .01^{**}$). A moderately strong correlation between normalized negative work was observed for lower leg muscles, albeit not significant ($R^2 = 0.46$, $p = .060$). The regression was subject to a large bias due to the peroneus, which, in line with the study of Hu and Blemker (2015), has a high fat fraction value and a low amount of normalized negative work during gait [16]. In contrast to Hu and Blemker (2015), the correlation was significant without excluding the adductor magnus in the upper leg from the analysis [16]. Generally, higher fat fractions are observed in muscles showing higher values of normalized negative work during gait.

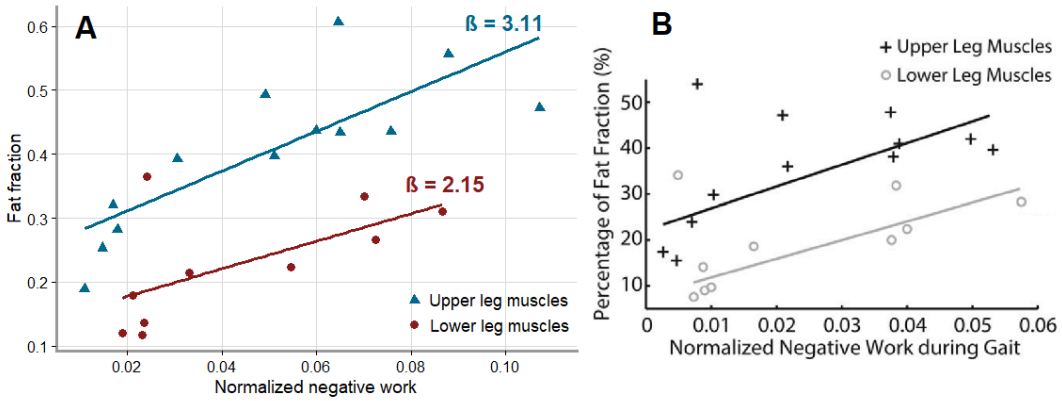

Figure 19: **A**: linear regression between normalized negative work and fat fraction values for upper and lower leg muscles separately. Slopes of the linear regression line are indicated with β. **B**: linear regression between normalized negative work and fat fraction values, adapted from Hu and Blemker (2015) [16].

A moderately strong correlation can be observed between normalized positive work and fat fraction values for upper leg muscles ($R^2 = 0.46$, $p < .05^*$), as illustrated in Figure 20A. This is in contrast with Hu and Blemker (2015), where no significant correlations were found between normalized positive work and fat fraction values for both upper and lower leg muscles, as illustrated in Figure 20B [16]. For lower leg muscles, a weak yet insignificant correlation between normalized positive work can be observed ($R^2 = 0.10$, $p = 0.36$).

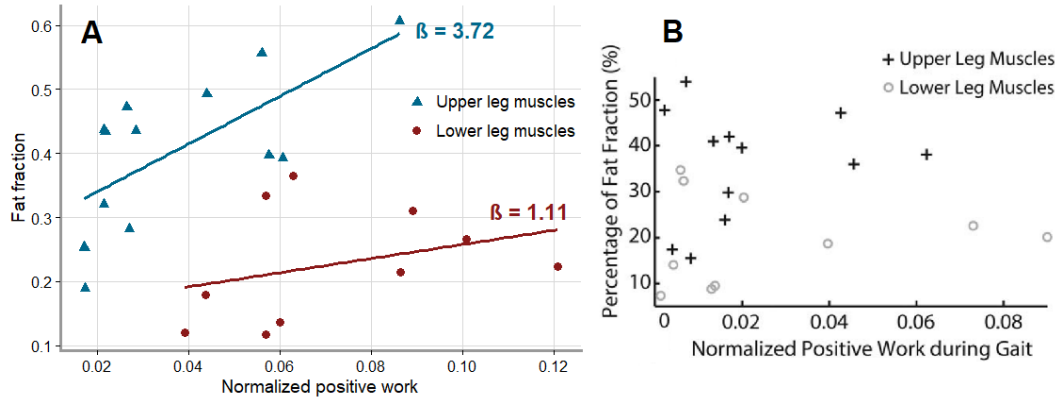

Figure 20: **A**: linear regression between normalized positive work and fat fraction values for upper and lower leg muscles separately. Slopes of the linear regression line are indicated with β. **B**: linear regression between normalized positive work and fat fraction values, adapted from Hu and Blemker (2015) [16].

From Figure 19, similarities in average normalized negative work values between upper and lower leg muscles can be observed. Average normalized positive work values are higher for lower leg muscles than for upper leg muscles, as can be observed from Figure 20. Still, fat fraction values are generally higher in upper leg muscles.

3.2 Extension Hu and Blemker (2015)

In this section, the logit transform of the fat fractions ($logFF$) was used in the linear models, see equations 9 and 10. An association between normalized negative work and $logFF$ was observed, with higher normalized negative work values corresponding to higher $logFF$ values (Table 3). The effect of leg part on $logFF$ was highly significant, indicating a higher predicted fat fraction for upper leg muscles than for lower leg muscles. The interaction $W_{neg,norm} \cdot Part$ was not significantly associated to $logFF$, which showed that the association between normalized negative work and $logFF$ was not significantly stronger for upper leg muscles than for lower leg muscles and vice versa.

Table 3: Output multiple-regression model of normalized negative work versus $logFF$: upper leg muscles versus lower leg muscles (eq.10).

	Estimate (β)	SE β	95% CI	p-value
$W_{neg,norm}$	13.456	4.943	3.768 - 23.144	.014*
$Part$	0.786	0.162	0.468 - 1.104	<.001*
$W_{neg,norm} \cdot Part$	0.306	6.117	-11.683 - 12.295	.961

The effect of normalized negative work on $logFF$ for both upper and lower leg muscles is shown in Figure 21, where $logFF$ was transformed back to fat fraction values.

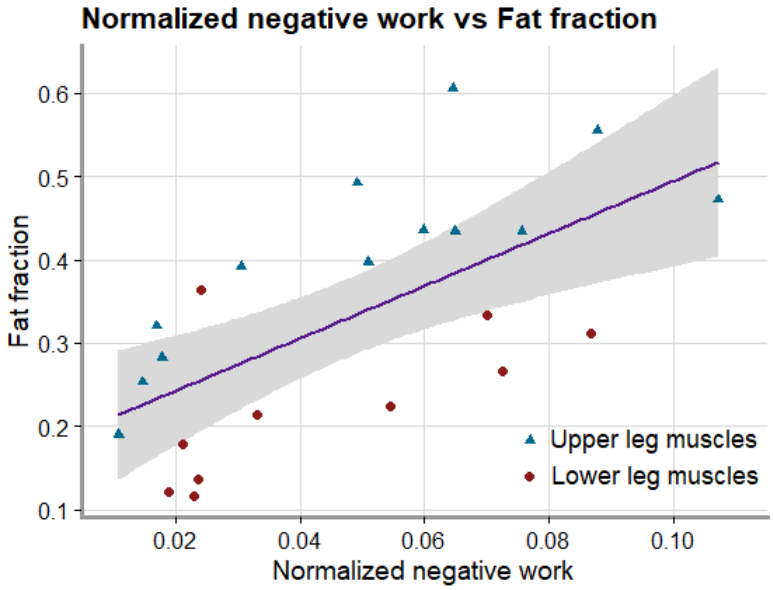

Figure 21: Normalized negative work was significantly associated with $logFF$ when upper and lower leg muscles are not separated. $logFF$ was transformed back to fat fraction values in the graph.

No significant association was observed between normalized positive work and $logFF$ (Table 4). In agreement with the previous analysis, the effect of leg part on $logFF$ was significant. The interaction $W_{pos,norm} \cdot Part$ was not significantly associated to $logFF$, which shows that the association between normalized positive work and $logFF$ is not significantly stronger for upper leg muscles than for lower leg muscles and vice versa. The effect of normalized absolute work, the sum of normalized negative and positive work, on $logFF$ is found in Appendix C.

Table 4: Output multiple-regression model of normalized positive work versus $logFF$: upper leg muscles versus lower leg muscles.

	Estimate (β)	SE β	95% CI	p-value
$W_{pos,norm}$	7.940	5.582	-3.000 - 18.881	.191
$Part$	1.281	0.244	0.803 - 1.759	<.001*
$W_{pos,norm}$·Part	8.287	8.523	-8.418 - 24.992	.343

3.3 Muscle architecture and negative work

Significant associations between both muscle architecture parameters (L_f and $PCSA$) and $logFF$ were observed. The interaction $L_f \cdot PCSA$ was also significant, which indicates that the effect of L_f on $logFF$ was stronger if $PCSA$ was larger (Table 5). Individual effects of $PCSA$ and L_f on $logFF$ are visualized in Figure 22, where $logFF$ was transformed back to fat fraction values.

Table 5: Output multiple-regression model of muscle architecture versus $logFF$ (eq.11).

	Estimate (β)	SE β	95% CI	p-value
L_f	0.098	0.030	0.039 - 0.157	.004*
$PCSA$	0.076	0.020	0.037 - 0.115	.001*
L_f·PCSA	0.015	0.005	0.005 - 0.024	.005*

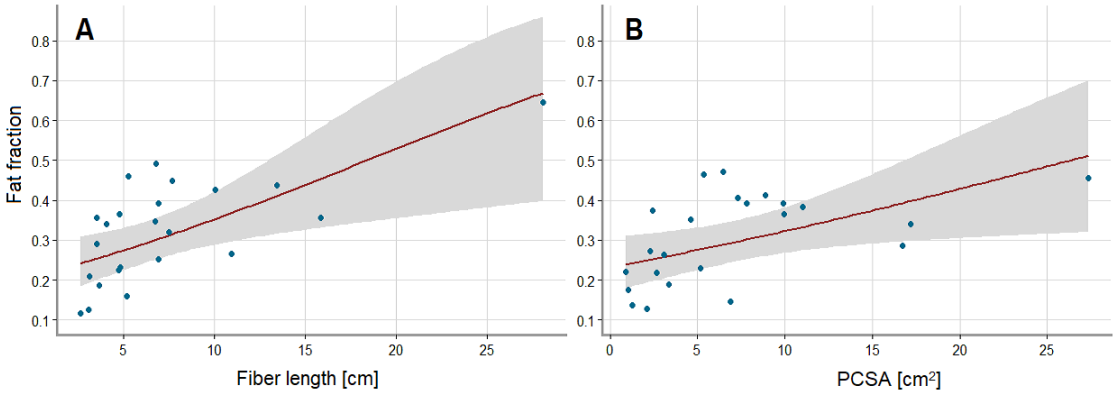

Figure 22: Both fiber length (Lf) and PCSA are associated with $logFF$.

Since the interaction $L_f \cdot PCSA$ was significantly associated with $logFF$, L_f and $PCSA$ were multiplied to acquire muscle volume (V_{mus}). An association between total negative work and $logFF$ was observed (Table 6). The interaction V_{mus}·W$_{neg,tot}$ was also significant, which indicates that the effect of total negative work on $logFF$ was weaker if V_{mus} was larger.

Table 6: Output multiple-regression model of total negative work versus $logFF$ (eq.12).

	Estimate (β)	SE β	95% CI	p-value
V_{mus}	0.011	0.002	[0.007, 0.014]	<.001*
$W_{neg,tot}$	0.195	0.090	[0.019, 0.371]	.043*
V_{mus}·W$_{neg,tot}$	-0.012	0.003	[-0.018, -0,006]	<.001*

The individual effects of V_{mus} and $W_{neg,tot}$ on $logFF$ are visualized Figure 23, where $logFF$ was transformed back to fat fraction values.

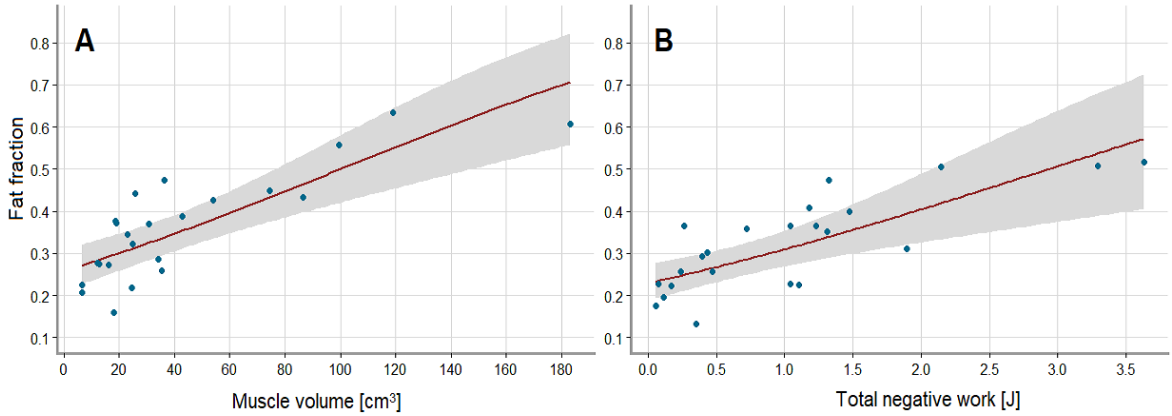

Figure 23: Both muscle volume (A) and total negative work (B) were significantly associated with fat replacement. $logFF$ was transformed back to fat fraction values in the graph.

Figure 24 shows the different effects of total negative work on $logFF$ for different in muscle volumes: small muscle volume (Fig. 24A), intermediate muscle volume (Fig. 24B) and large muscle volume (Fig. 24C). The effect of total negative work on $logFF$ was stronger if muscle volume was lower. For large muscle volumes, a negative association between total negative work and $logFF$ was observed.

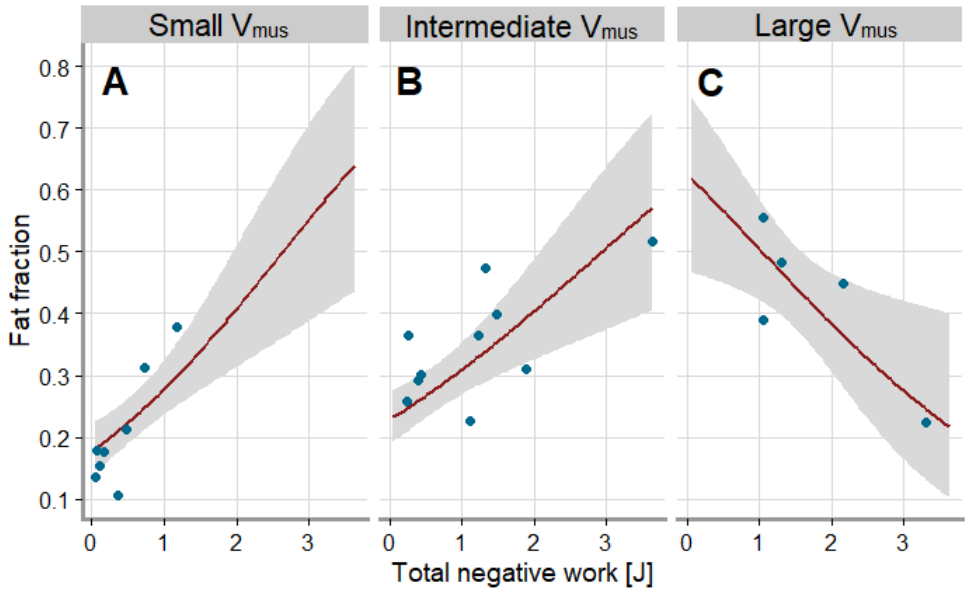

Figure 24: Different effects of total negative work on muscle fat fractions for: **A)** small muscle volumes, **B)** intermediate muscle volumes and **C)** large muscle volumes. $logFF$ was transformed back to fat fraction values in the graph.

4 Discussion

4.1 Eccentric contraction during gait is associated with fat replacement in DMD

The results of this study show that eccentric contraction is associated with fat replacement in leg muscles of DMD patients. Two goals were defined in this study. The first goal was to apply the method of Hu and Blemker (2015), in which linear regressions between fat fractions and normalized negative and positive work values were analyzed for upper and lower leg muscles separately to multiple gait cycles of multiple children [16]. A large difference in average normalized work values was found between studies, where the values of this study were on average almost twice as high. This difference may partly be explained by increased normalized walking speed of the subjects, since it affects joint power and muscle activity [61, 62]. In this study the normalized walking speed was 0.53, which can be considered fast [61]. The non-normalized walking speeds of this study were on average already higher than the reported walking speed of the subject analyzed by Hu and Blemker (2015) (1.45 versus 1.36) [16]. Therefore, average normalized walking speed was certainly higher in this study. Since differences in normalized work values are so large between studies, it is likely that they are partly caused by scaling of muscle fiber length and maximal isometric force, which directly affect normalized work values.

The order of normalized negative work values was generally agreeable between studies, except for the rectus femoris and adductor magnus. Various gait parameters and muscle activity patterns respond differently to increasing walking speed. As such, the rectus femoris is said to be essentially non-active at slower walking speeds, while activation rapidly increases for faster walking speeds [61], which explains why it showed the highest normalized negative work value in this study, in contrast to Hu and Blemker (2015) [16]. Interestingly, in the study of Hu and Blemker (2015) the adductor magnus was excluded to find a significant correlation between normalized negative work values and fat fractions. A similar sensitivity to normalized walking speed may also apply for the adductor magnus, although quantification of its contribution during gait is relatively understudied [76]. However, one study found that the adductor magnus was already one of the most active muscles during gait at comfortable walking speed, as quantified by volumetric uptake of a glucose analog [77].

To find a significant correlation between normalized negative work and fat fraction values in the lower leg, Hu and Blemker (2015) excluded the peroneus from the regression analysis. Although the position of the peroneus in the order of normalized negative work values was different in this study, its inclusion still did not result in a significant correlation due to a high fat fraction value and a low amount of normalized negative work during gait. Therefore, an explanation for the high fat fraction of the peroneus was not found in this study, although another study observed increased activity of the peroneus for very slow walking speeds, which indicates that the activity of this muscle is associated to achieving postural stability rather than to achieve locomotion [78]. As young children learn to stand up, this is initially associated with postural instability. Furthermore, postural instability is even more present in DMD, and it will remain to be in the rest of their ambulant lives. Therefore, early involvement of the peroneus in DMD may be related to increased loading of this muscle as children learn to stand up and maintain balance.

To summarize the first part of the results, both normalized negative and positive work showed significant correlations with fat fractions for upper leg muscles. A relation between normalized positive work and fat replacement was not expected since it is believed that eccentric contraction,

not concentric contraction, is especially harmful for dystrophin-absent muscle. Also, this result was not expected since it is in contrast to Hu and Blemker (2015) [16]. No significant relation was observed between normalized negative work and fat fractions for lower leg muscles, except when the peroneus was excluded from the analysis, which is in line with Hu and Blemker (2015) [16]. As expected, no significant relation between normalized positive work and fat fractions were observed for lower leg muscles. Furthermore, although upper and lower leg muscles showed similar average values of normalized negative and positive work, fat fractions were generally higher in upper leg muscles.

The second goal of this study was to extend the analysis by evaluating the effect of leg part (upper or lower) on fat replacement and (2) to analyze separate effects of muscle architecture and total negative work on fat replacement. In the second section of the results, normalized negative work was significantly associated with $logFF$, where higher normalized negative work values corresponded to higher $logFF$. In contrast, no significant association between normalized positive work and $logFF$ was found. The effect of leg part was highly significant, which indicates that upper leg muscles are stronger predictors for fat replacement than lower leg muscles. This is in line with a frequently observed proximal-to-distal gradient of muscle weakness in DMD. However, the interaction $W_{neg,norm} \cdot Part$ was not significant, suggesting that the effect of normalized negative work on $logFF$ was not stronger for upper leg muscles than for lower leg muscles. A possible explanation why upper leg muscles are affected earlier in DMD, and thus have higher fat fractions, is that decreased ankle power is observed in children < 7 years old [57], which is compensated for by increased hip power [60]. It is hypothesized that such kinetic differences in children of age < 7 reflect neuromuscular immaturity. In other words, proximal muscles associated with generating hip power may be subject to relatively higher amounts of negative work than distal muscles associated with generating ankle power in young children. The crawling phase may also play a role in a proximal-to-distal gradient of muscle weakness in DMD, since larger hip flexion/extension angles are found during this motion than during gait [79], which arguably results in relatively larger hip moments and thus power of muscles associated with this motion. Similarly, other physical activities than gait, such as stair walking or running, may contribute to a proximal-to-distal gradient in muscle weakness as well.

Significant associations were observed between $logFF$ and muscle architecture parameters L_f and $PCSA$. Furthermore, in agreement to Veeger et al. (2021), the interaction $L_f \cdot PCSA$ was significantly associated with $logFF$ [55]. Therefore, muscle architecture parameters L_f and $PCSA$ were multiplied to calculate muscle volume, which, along with total negative work ($W_{neg,tot}$), was used as independent variable in the subsequent analysis to predict fat replacement. Total negative work was significantly associated to $logFF$, which indicates that although muscle architecture is strongly associated with fat replacement, eccentric contraction contributes to fat replacement as well. A negative association between the interaction $V_{mus} \cdot W_{neg,tot}$ and $logFF$ was observed, indicating that the effect of total negative work on $logFF$ is weaker for muscles with larger muscle volumes. This was expected since muscles with larger volumes are able to generate more power, and are therefore less taxed than muscles generating the same amount of power with less volume.

A negative association between total negative work and $logFF$ was observed for muscles with large muscle volumes (Figure 24C), which was not expected. This effect was based on only five muscles with large volumes, the gluteus maximus, vastus lateralis, adductor magnus, soleus and vastus medialis, in which especially one observation, the soleus, resulted in the observed negative association. In *mdx* mice, it was found that especially muscles consisting of fast-twitch fibers are susceptible to eccentric contraction induced damage, whereas the soleus consists primarily of slow-twitch fibers [42]. One study found that the dystrophic pathology in the soleus muscle is diminished due to overexpression of the neuronal nitric oxide synthase (nNOS) transgene, thereby providing nitric oxide as anti-inflammatory molecule [80]. Another study demonstrated that the slow-twitch

soleus muscle in *mdx* mice is no more susceptible to eccentric contraction induced damage than for age-matched controls, showing reduced amounts of branched fibers than in other muscles [81]. Fiber type compositions are more complex in humans than in mice [82], although with an average of 80%, the human soleus predominantly contains slow-twitch fibers as well [83]. Such findings suggest that the soleus, at least in *mdx* mice, is designed to regenerate better after damage than other leg muscles.

4.2 Limitations

This study is an extension of the preliminary study published by Hu and Blemker (2015) [16]. Some of the study limitations that they addressed have been resolved, but not all.

One limitation they addressed was that the gait analysis was based on an unimpaired adult man, while DMD patients never develop a healthy adult gait pattern. Furthermore, although walking is one of the most common daily activities, other types of physical activities may also contribute to muscle degeneration [16], which were neglected in this study. For this study it was chosen to analyze gait of unimpaired young children, since their muscle contributions reflect best which muscles are initially affected by eccentric contraction in DMD. The mean age of this cross-sectional sample of children was slightly above 7, while the mean age would have been preferred to be lower, such that the kinetics would reflect those of relatively unimpaired DMD patients. Gait of one DMD patient was analyzed to explore differences in muscle contributions due to gait deviation, which resulted in small differences in normalized work values, as illustrated in the graphs found in Appendix D.

Another limitation of this study is the fact that the same musculoskeletal model was used as Hu and Blemker (2015) [16, 50]. While this was a logical choice in order to compare results when their method was applied to multiple gait cycles of multiple children, it would also be meaningful to explore possible effects of using a different, scientifically valid model to calculate muscle contributions. Model parameters can be slightly different in bone geometry, muscle architecture and alignment, and they may use a different muscle model, all of which affect the predicted work of muscles during gait. Furthermore, the Vicon Plug-in-Gait model was used to process the data, which contains numerous simplifications with regard to calculating joint centers, introducing both random and systemic errors [84]. For example, hip joint centers are derived from regression equations, with coefficients obtained from using imaging techniques on living adult males or direct measurements of cadavers [85].

Also, the muscle models used in this study were based on a healthy population and highly simplified [86]. Detailed stress-strain distributions within muscles can therefore not be simulated with high detail, as already addressed by Hu and Blemker (2015) [16]. To accurately model DMD gait and calculate associated muscle contributions, a model with subject-specific anthropometrics and muscle mechanical properties should be developed.

Lastly, fat fraction values were extracted from the LUMC database and from Wokke et al. (2014) [10], and were subsequently added together to acquire fat fraction values of 32 DMD patients. A golden standard to quantify fat fractions has not yet been established. Therefore, the order of muscle fat fractions used in this study is probably not totally accurate. Moreover, fat fractions in DMD are not solely dependent on fat replacement, since muscles of DMD patients show changes in cross-sectional area (CSA). For example, atrophy of the contractile CSA of the adductor magnus [8, 17, 28], quadriceps [10, 17, 24], biceps femoris [10, 17, 24] and gluteus muscles [24] has been reported. In contrast, hypertrophy of the contractile CSA of the gracilis [24, 28], sartorius [24, 28], and triceps surae [10, 24] is frequently seen. Therefore, the amount of fat replacement may in some cases be overestimated for atrophied muscles, or underestimated for hypertrophied muscles.

4.3 Future work

Future recommendations include analyzing other physical activities of unimpaired children than gait, such as crawling, stair walking or running. It may be that certain types of activities result in relatively higher amounts of (normalized) negative work in upper leg muscles with respect to lower leg muscles. Higher fat fractions are generally found in proximal muscles, while average normalized negative work values were similar between upper and lower leg muscles. Therefore, in this study no explanation was found for the differences in fat fractions between upper and lower leg muscles. Similarly, an explanation of the high fat fraction of the peroneus in the lower leg was not found, while it was mentioned that its activity increases for very slow walking speeds [78]. Therefore, it is also recommended to analyze very slow walking speeds or balancing tests.

Furthermore, accurate models of DMD patients with subject-specific anthropometrics and muscle mechanical properties that reflect muscle contraction patterns of dystrophic muscles should be developed. This way, pathological changes that reflect the different progressions of muscle degeneration can be validated. That is, if subject-specific longitudinal muscle MRI data and 3D gait analysis data are available, along with muscle models that can accurately reflect altered mechanical properties related to the structural and compositional changes observed in muscles of DMD patients.

Also, as addressed by Hu and Blemker (2015), finite element 3D muscle models that reveal stress-strain distributions within muscles should be incorporated into simulation. This way, the effect of different muscle architecture and geometry on non-uniform stress distributions within muscles can be evaluated [16]. Elevated stress-strain concentrations are usually found near the myotendinous junction, where dystrophin is normally abundant [40, 87]. Muscle fat replacement also develops non-uniformly, with higher fat fractions found near the myotendinous junction with respect to the muscle belly [88]. Also, the same type of contraction may result in different levels of stress-strain concentrations among muscles. Taken together, incorporating detailed finite element muscle models in gait simulation may provide insight regarding varying degrees of muscle damage in DMD after eccentric contraction.

4.4 Conclusion

In conclusion, the results of this study show that eccentric contraction during gait is associated with muscle fat replacement in DMD patients. Accounting for the effect of muscle architecture, the effect of negative work on muscle fat replacement was still significant. However, the fact that fat fractions in upper leg muscles are generally higher than in lower leg muscles cannot be explained from these results. The high fat fraction of the peroneus also remains a matter to be resolved in future studies. More insight regarding the proximal-to-distal gradient of muscle degeneration in DMD may be generated if gait of an even younger cross-sectional sample of unimpaired children is analyzed, or if other activities than walking are simulated. Further understanding of the process of muscle degeneration in DMD may be established if models with subject-specific anthropometrics and biomechanics are developed, and if finite element 3D muscle models are incorporated into musculoskeletal simulation. Ultimately, they can potentially generate more insight into effects of various types of exercise on muscle damage in DMD. The effect of exercise on prolonged muscle function preservation remains controversial, but in agreement with most of the literature, exercises including eccentric contraction should be avoided.

References

[1] J. K. Mah, "Current and emerging treatment strategies for Duchenne muscular dystrophy," *Neuropsychiatric Disease and Treatment*, vol. 12, no. 1, pp. 1795–1807, 2016.

[2] D. G. Allen, N. P. Whitehead, and S. C. Froehner, "Absence of Dystrophin Disrupts Skeletal Muscle Signaling: Roles of Ca 2+ , Reactive Oxygen Species, and Nitric Oxide in the Development of Muscular Dystrophy," *Physiological Reviews*, vol. 96, no. 1, pp. 253–305, 2015.

[3] D. J. Birnkrant, K. Bushby, C. M. Bann, S. D. Apkon, A. Blackwell, D. Brumbaugh, L. E. Case, P. R. Clemens, S. Hadjiyannakis, S. Pandya, N. Street, J. Tomezsko, K. R. Wagner, L. M. Ward, and D. R. Weber, "Diagnosis and management of Duchenne muscular dystrophy, part 1: diagnosis, and neuromuscular, rehabilitation, endocrine, and gastrointestinal and nutritional management," *The Lancet Neurology*, vol. 17, no. 3, pp. 251–267, 2018.

[4] E. Ciafaloni, A. Kumar, K. Liu, S. Pandya, C. Westfield, J. Deborah, K. M. C. Conway, C. Cunniff, K. Mathews, P. A. Romitti, M. P. Mcdermott, I. City, and C. Medical, "Age at onset of first signs or symptoms predicts age at loss of ambulation in Duchenne and Becker Muscular Dystrophy: Data from the MD STARnet," *J Pediatr Rehabil Med.*, vol. 9, no. 1, pp. 5–11, 2018.

[5] J. Burakiewicz, C. D. Sinclair, D. Fischer, G. A. Walter, H. E. Kan, and K. G. Hollingsworth, "Quantifying fat replacement of muscle by quantitative MRI in muscular dystrophy," *Journal of Neurology*, vol. 264, no. 1, pp. 2053–2067, 2017.

[6] J. H. Johnston, H. K. Kim, A. C. Merrow, T. Laor, S. Serai, P. S. Horn, D. H. Kim, and B. L. Wong, "Quantitative Skeletal Muscle MRI: Part 1, Derived T2 Fat Map in Differentiation Between Boys With Duchenne Muscular Dystrophy and Healthy Boys," *American Journal of Roentgenology*, vol. 205, 2015.

[7] M. Gaeta, S. Messina, A. Mileto, G. L. Vita, G. Ascenti, S. Vinci, A. Bottari, G. Vita, N. Settineri, D. Bruschetta, S. Racchiusa, and F. Minutoli, "Muscle fat-fraction and mapping in Duchenne muscular dystrophy: evaluation of disease distribution and correlation with clinical assessments," *Skeletal Radiology*, vol. 41, no. 1, pp. 955–961, 2012.

[8] L. Yin, Z. Y. Xie, H. Y. Xu, S. S. Zheng, Z. X. Wang, J. X. Xiao, and Y. Yuan, "T2 Mapping and Fat Quantification of Thigh Muscles in Children with Duchenne Muscular Dystrophy," *Current medical science*, vol. 39, no. 1, pp. 138–145, 2019.

[9] E. Mercuri, A. Pichiecchio, J. Allsop, S. Messina, M. Pane, and F. Muntoni, "Muscle MRI in inherited neuromuscular disorders: Past, present, and future," *Journal of Magnetic Resonance Imaging*, vol. 25, no. 2, pp. 433–440, 2007.

[10] B. Wokke, J. Van den Bergen, M. Versluis, E. Niks, J. Milles, A. Webb, E. van Zwet, A. Aartsma-Rus, J. Verschuuren, and H. Kan, "Quantitative MRI and strength measurements in the assessment of muscle quality in Duchenne muscular dystrophy," *Neuromuscular Disorders*, vol. 24, no. 1, pp. 409–416, 2014.

[11] N. Deconinck and B. Dan, "Pathophysiology of Duchenne Muscular Dystrophy: Current Hypotheses," *Pediatric Neurology*, vol. 36, no. 1, pp. 1–7, 2007.

[12] L. Uttley, J. Carlton, H. B. Woods, and J. Brazier, "A review of quality of life themes in Duchenne muscular dystrophy for patients and carers," *Health and Quality of Life Outcomes*, vol. 16, no. 1, pp. 1–16, 2018.

[13] M. F. Jacques, G. L. Onambele-Pearson, N. D. Reeves, G. K. Stebbings, J. Smith, and C. I. Morse, "Relationships between muscle size, strength, and physical activity in adults with muscular dystrophy," *Journal of Cachexia, Sarcopenia and Muscle*, vol. 9, no. 1, pp. 1042–1052, 2018.

[14] B. Kogelman, K. Putker, M. Hulsker, C. Tanganyika-de Winter, L. Van der Weerd, A. Aartsma-Rus, and M. Van Putten, "Voluntary exercise improves muscle function and does not exacerbate muscle and heart pathology in aged Duchenne muscular dystrophy mice," *Journal of Molecular and Cellular Cardiology*, vol. 125, no. 1, pp. 29–38, 2018.

[15] A. Seth, J. L. Hicks, T. K. Uchida, A. Habib, C. L. Dembia, J. J. Dunne, C. F. Ong, M. S. DeMers, A. Rajagopal, M. Millard, S. R. Hamner, E. M. Arnold, J. R. Yong, S. K. Lakshmikanth, M. A. Sherman, J. P. Ku, and S. Delp, "OpenSim: Simulating musculoskeletal dynamics and neuromuscular control to study human and animal movement," *Computational Biology*, vol. 14, no. 7, 2018.

[16] X. Hu and S. S. Blemker, "Musculoskeletal simulation can help explain selective muscle degeneration in Duchenne muscular dystrophy," *Muscle and Nerve*, vol. 52, no. 1, pp. 174–182, 2015.

[17] H. Akima, D. Lott, C. Senesac, J. Deol, S. Germain, I. Arpan, R. Bendixen, H. L. Sweeney, G. Walter, and K. Vandenborne, "Relationships of thigh muscle contractile and non-contractile tissue with function, strength, and age in boys with Duchenne muscular dystrophy," *Neuromus*, vol. 22, no. 1, pp. 16–25, 2012.

[18] T. A. Wren, S. Bluml, L. Tseng-Ong, and V. Gilsanz, "Three-point technique of fat quantification of muscle tissue as a marker of disease progression in Duchenne muscular dystrophy: preliminary study.," *AJR. American journal of roentgenology*, vol. 190, no. January 2008, 2008.

[19] A. M. Barnard, R. J. Willcocks, E. L. Finanger, M. J. Daniels, W. T. Triplett, W. D. Rooney, D. J. Lott, S. C. Forbes, D. J. Wang, C. R. Senesac, A. T. Harrington, R. S. Finkel, B. S. Russman, B. J. Byrne, G. I. Tennekoon, G. A. Walter, H. L. Sweeney, and K. Vandenborne, "Skeletal muscle magnetic resonance biomarkers correlate with function and sentinel events in Duchenne muscular dystrophy," *PLoS ONE*, vol. 13, no. 3, 2018.

[20] W. D. Rooney, Y. A. Berlow, W. T. Triplett, S. C. Forbes, R. J. Willcocks, D. J. Wang, I. Arpan, H. Arora, C. Senesac, D. J. Lott, G. Tennekoon, R. Finkel, B. S. Russman, E. L. Finanger, S. Chakraborty, E. O'Brien, B. Moloney, A. Barnard, H. L. Sweeney, M. J. Daniels, G. A. Walter, and K. Vandenborne, "Modeling disease trajectory in Duchenne muscular dystrophy," *Neurology*, vol. 94, no. 15, pp. E1622–E1633, 2020.

[21] K. J. Naarding, H. Reyngoudt, E. W. Van Zwet, M. T. Hooijmans, C. Tian, I. Rybalsky, K. C. Shellenbarger, J. Le Louër, B. L. Wong, P. G. Carlier, H. E. Kan, and E. H. Niks, "MRI vastus lateralis fat fraction predicts loss of ambulation in Duchenne muscular dystrophy," *Neurology*, vol. 94, no. 13, pp. E1386–E1394, 2020.

[22] A. Mankodi, C. A. Bishop, S. Auh, R. D. Newbould, K. H. Fischbeck, and R. L. Janiczek, "Quantifying disease activity in fatty-infiltrated skeletal muscle by IDEAL-CPMG in Duchenne muscular dystrophy," *Neuromuscular Disorders*, vol. 26, no. 1, pp. 650–658, 2016.

[23] S. Ponrartana, L. Ramos-Platt, T. A. L. Wren, H. H. Hu, T. G. Perkins, J. M. Chia, and V. Gilsanz, "Effectiveness of diffusion tensor imaging in assessing disease severity in Duchenne muscular dystrophy: preliminary study," *Pediatric Radiology*, vol. 45, no. 4, pp. 582–589, 2015.

[24] C. Godi, A. Ambrosi, F. Nicastro, S. C. Previtali, C. Santarosa, S. Napolitano, A. Iadanza, M. Scarlato, M. G. Natali Sora, A. Tettamanti, S. Gerevini, M. P. Cicalese, C. Sitzia, M. Venturini, A. Falini, R. Gatti, F. Ciceri, G. Cossu, Y. Torrente, and L. S. Politi, "Longitudinal MRI quantification of muscle degeneration in Duchenne muscular dystrophy," *Annals of Clinical and Translational Neurology*, vol. 3, no. 8, pp. 607–622, 2016.

[25] K. Polavarapu, M. Manjunath, V. Preethish-Kumar, D. Sekar, S. Vengalil, P. T. Thomas, T. N. Sathyaprabha, R. D. Bharath, and A. Nalini, "Muscle MRI in Duchenne muscular dystrophy: Evidence of a distinctive pattern," *Neuromuscular Disorders*, vol. 26, no. 11, pp. 768–774, 2016.

[26] H. K. Kim, T. Laor, P. S. Horn, J. M. Racadio, B. Wong, and B. J. Dardzinski, "T2 Mapping in Duchenne Muscular Dystrophy: Distribution of Disease Activity and Correlation with Clinical Assessments," *Radiology*, vol. 255, no. 3, pp. 899–908, 2010.

[27] W. Li, Y. Zheng, W. Zhang, Z. Wang, J. Xiao, and Y. Yuan, "Progression and variation of fatty infiltration of the thigh muscles in Duchenne muscular dystrophy, a muscle magnetic resonance imaging study," *Neuromuscular Disorders*, vol. 25, no. 1, pp. 375–380, 2015.

[28] F. A. Marden, A. M. Connolly, M. J. Siegel, and D. A. Rubin, "Compositional analysis of muscle in boys with Duchenne muscular dystrophy using MR imaging," *Skeletal Radiology*, vol. 34, no. 1, pp. 140–148, 2005.

[29] J. K. Deisch, *Muscle and Nerve Development in Health and Disease*, vol. 4. Elsevier Inc., sixth edit ed., 2017.

[30] J. D. Gumerson and D. E. Michele, "The dystrophin-glycoprotein complex in the prevention of muscle damage," *Journal of Biomedicine and Biotechnology*, vol. 2011, 2011.

[31] K. S. Ramaswamy, M. L. Palmer, J. H. Van Der Meulen, A. Renoux, T. Y. Kostrominova, D. E. Michele, and J. A. Faulkner, "Lateral transmission of force is impaired in skeletal muscles of dystrophic mice and very old rats," *Journal of Physiology*, vol. 589, no. 5, pp. 1195–1208, 2011.

[32] J. Feher, *Quantitative Human Physiology (Second Edition)*. 2017.

[33] D. R. Claflin and S. V. Brooks, "Direct observation of failing fibers in muscles of dystrophic mice provides mechanistic insight into muscular dystrophy," *American Journal of Physiology-Cell Physiology*, vol. 294, no. 1, pp. 651–658, 2008.

[34] S. Hody, J. L. Croisier, T. Bury, B. Rogister, and P. Leprince, "Eccentric muscle contractions: Risks and benefits," *Frontiers in Physiology*, vol. 10, no. MAY, pp. 1–18, 2019.

[35] B. J. Petrof, "The molecular basis of activity-induced muscle injury in Duchenne muscular dystrophy," *Molecular and Cellular Biochemistry*, vol. 179, no. 1, pp. 111–123, 1998.

[36] H. H. Stedman, H. L. Sweeney, A. M. Kelly, J. B. Shrager, and B. J. Petrof, "Dystrophin protects the sarcolemma from stresses developed during muscle contraction.," *Proceedings of the National Academy of Sciences*, vol. 90, no. April 1993, pp. 3710–3714, 1993.

[37] C. A. Ottenheijm, A. M. Knottnerus, D. Buck, X. Luo, K. Greer, A. Hoying, S. Labeit, and H. Granzier, "Tuning passive mechanics through differential splicing of titin during skeletal muscle development," *Biophysical Journal*, vol. 97, no. 8, pp. 2277–2286, 2009.

[38] G. S. Lynch, J. A. Rafael, J. S. Chamberlain, and J. A. Faulkner, "Contraction-induced injury to single permeabilized muscle fibers from mdx, transgenic mdx, and control mice," *Am J Physiol Cell Physiol*, vol. 279, pp. 1290–1294, 2000.

[39] S. V. Brooks, E. Zerba, and J. A. Faulkner, "Injury to muscle fibres after single stretches of passive and maximally stimulated muscles in mice," vol. 488, no. 2, pp. 459–469, 1995.

[40] T. J. Byers, L. M. Kunkel, and S. C. Watkins, "The subcellular distribution of dystrophin in mouse skeletal, cardiac, and smooth muscle," *Journal of Cell Biology*, vol. 115, no. 2, pp. 411–421, 1991.

[41] J. A. Call, G. L. Warren, M. Verma, and D. A. Lowe, "Acute failure of action potential conduction in mdx muscle reveals new mechanism of contraction-induced force loss," *Journal of Physiology*, vol. 591, no. 15, pp. 3765–3776, 2013.

[42] S. Chan and S. I. Head, "The role of branched fibres in the pathogenesis of Duchenne muscular dystrophy," *Experimental Physiology*, vol. 96, no. 6, pp. 564–571, 2011.

[43] S. I. Head, D. A. Williams, and D. G. Stephenson, "Abnormalities in structure and function of limb skeletal muscle fibres of dystrophic mdx mice," *Proceedings of the Royal Society B: Biological Sciences*, vol. 248, no. 1322, pp. 163–169, 1992.

[44] W. R. Frontera and J. Ochala, "Skeletal Muscle: A Brief Review of Structure and Function," *Behavior Genetics*, vol. 45, no. 2, pp. 183–195, 2015.

[45] R. Qaisar, S. Bhaskaran, and H. Van Remmen, "Muscle fiber type diversification during exercise and regeneration," *Free Radical Biology and Medicine*, vol. 98, no. 1, pp. 56–67, 2016.

[46] L. Lacourpaille, F. Hug, A. Guével, Y. Péréon, A. Magot, J.-Y. Hogrel, and A. Nordez, "New insights on contraction efficiency in patients with Duchenne muscular dystrophy," *Journal of Applied Physiology*, vol. 117, no. 1, pp. 658–662, 2014.

[47] F. Hug, A. Magot, Y. Péréon, R. Gross, L. Lacourpaille, A. Guével, J.-Y. Hogrel, and A. Nordez, "Effects of Duchenne muscular dystrophy on muscle stiffness and response to electrically-induced muscle contraction: A 12-month follow-up," *Neuromuscular Disorders*, vol. 27, no. 1, pp. 214–220, 2017.

[48] G. Massey, P. Evangelidis, and J. Folland, "Influence of contractile force on the architecture and morphology of the quadriceps femoris," *Experimental Physiology*, vol. 100, no. 11, pp. 1342–1351, 2015.

[49] S. L. Delp, F. C. Anderson, A. S. Arnold, P. Loan, A. Habib, C. T. John, E. Guendelman, and D. G. Thelen, "OpenSim: open-source software to create and analyze dynamic simulations of movement.," *IEEE Trans Biomed Eng*, vol. 54, no. 11, pp. 1940–1950, 2007.

[50] C. T. John, F. C. Anderson, J. S. Higginson, and S. L. Delp, "Stabilisation of walking by intrinsic muscle properties revealed in a three-dimensional muscle-driven simulation," *Computer Methods in Biomechanics and Biomedical Engineering*, vol. 16, no. 4, pp. 451–462, 2013.

[51] L. Doglio, E. Pavan, I. Pernigotti, P. Petralia, C. Frigo, and C. Minetti, "Early signs of gait deviation in Duchenne muscular dystrophy," *European Journal of Physical and Rehabilitation Medicine*, vol. 47, no. 1, pp. 587–594, 2011.

[52] M. G. D'Angelo, M. Berti, L. Piccinini, M. Romei, M. Guglieri, S. Bonato, A. Degrate, A. C. Turconi, and N. Bresolin, "Gait pattern in Duchenne muscular dystrophy," *Gait and Posture*, vol. 29, no. 1, pp. 36–41, 2009.

[53] S. Sienko Thomas, C. E. Buckon, A. Nicorici, A. Bagley, C. M. McDonald, and M. D. Sussman, "Classification of the gait patterns of boys with Duchenne muscular dystrophy and their relationship to function," *Journal of Child Neurology*, vol. 25, no. 9, pp. 1103–1109, 2010.

[54] N. Gaudreault, D. Gravel, S. Nadeau, S. Houde, and D. Gagnon, "Gait patterns comparison of children with Duchenne muscular dystrophy to those of control subjects considering the effect of gait velocity," *Gait and Posture*, vol. 32, pp. 342–347, 2010.

[55] v. Z. E. a. M. D. e. a. Veeger, TTJ, "Muscle architecture is associated with muscle fat replacement in Duchenne and Becker muscular dystrophies," *Muscle & Nerve*, vol. 64, no. 5, pp. 576–584, 2021.

[56] U. Trinler, H. Schwameder, R. Baker, and N. Alexander, "Muscle force estimation in clinical gait analysis using AnyBody and OpenSim," *Journal of Biomechanics*, vol. 86, pp. 55–63, 2019.

[57] K. J. Ganley and C. M. Powers, "Gait kinematics and kinetics of 7-year-old children: A comparison to adults using age-specific anthropometric data," *Gait and Posture*, vol. 21, no. 2, pp. 141–145, 2005.

[58] K. J. Ganley and C. M. Powers, "Intersegmental dynamics during the swing phase of gait: A comparison of knee kinetics between 7 year-old children and adults," *Gait and Posture*, vol. 23, no. 4, pp. 499–504, 2006.

[59] V. L. Chester, M. Tingley, and E. N. Biden, "A comparison of kinetic gait parameters for 3-13 year olds," *Clinical Biomechanics*, vol. 21, no. 7, pp. 726–732, 2006.

[60] D. Sutherland, "The development of mature gait," *Gait and Posture*, vol. 6, no. 2, pp. 163–170, 1997.

[61] M. H. Schwartz, A. Rozumalski, and J. P. Trost, "The effect of walking speed on the gait of typically developing children," *Journal of Biomechanics*, vol. 41, no. 8, pp. 1639–1650, 2008.

[62] A. L. Hof, H. Elzinga, W. Grimmius, and J. P. Halbertsma, "Speed dependence of averaged EMG profiles in walking," *Gait and Posture*, vol. 16, no. 1, pp. 78–86, 2002.

[63] A. S. Cheung, H. Gray, A. G. Schache, R. Hoermann, D. Lim Joon, J. D. Zajac, M. G. Pandy, and M. Grossmann, "Androgen deprivation causes selective deficits in the biomechanical leg muscle function of men during walking: a prospective case–control study," *Journal of Cachexia, Sarcopenia and Muscle*, vol. 8, no. 1, pp. 102–112, 2017.

[64] A. L. Hof, "Scaling gait data to body size," *Gait and Posture*, vol. 4, no. 3, pp. 222–223, 1996.

[65] M. Goudriaan, M. Van den Hauwe, C. Simon-Martinez, C. Huenaerts, G. Molenaers, N. Goemans, and K. Desloovere, "Gait deviations in Duchenne muscular dystrophy—Part 2. Statistical non-parametric mapping to analyze gait deviations in children with Duchenne muscular dystrophy," *Gait and Posture*, vol. 63, no. 1, pp. 159–164, 2018.

[66] I. Vandekerckhove, N. de Beukelaer, M. van den Hauwe, B. R. Shuman, K. M. Steele, A. van Campenhout, N. Goemans, K. Desloovere, and M. Goudriaan, "Muscle weakness has a limited effect on motor control of gait in Duchenne muscular dystrophy," *PLoS ONE*, vol. 15, no. 9 September 2020, pp. 1–15, 2020.

[67] S. R. Ward, C. M. Eng, L. H. Smallwood, and R. L. Lieber, "Are current measurements of lower extremity muscle architecture accurate?," *Clin Orthop Relat Res.*, vol. 467, no. 4, pp. 1074–1082, 2009.

[68] E. M. Arnold, S. R. Hamner, A. Seth, M. Millard, and S. L. Delp, "How muscle fiber lengths and velocities affect muscle force generation as humans walk and run at different speeds," *Journal of Experimental Biology*, vol. 216, no. 11, pp. 2150–2160, 2013.

[69] T. L. Wickiewicz, R. R. Roy, P. L. Powell, and V. R. Edgerton, "Muscle architectuie of the human lower limb," *Clin. Orthop. Rei. Res.*, vol. 179, pp. 275–283, 1983.

[70] J. A. Friederich and R. A. Brand, "Muscle fiber architecture in the human lower limb," *J. Biomechanics*, vol. 23, no. 1, pp. 91–95, 1990.

[71] K. Veerkamp, W. Schallig, J. Harlaar, C. Pizzolato, C. P. Carty, D. G. Lloyd, and M. M. van der Krogt, "The effects of electromyography-assisted modelling in estimating musculotendon forces during gait in children with cerebral palsy," *Journal of Biomechanics*, vol. 92, no. xxxx, pp. 45–53, 2019.

[72] D. G. Thelen and F. C. Anderson, "Using computed muscle control to generate forward dynamic simulations of human walking from experimental data," *Journal of Biomechanics*, vol. 39, no. 6, pp. 1107–1115, 2006.

[73] E. de Vlugt, S. van Eesbeek, P. Baines, J. Hilte, C. G. Meskers, and J. H. de Groot, "Short range stiffness elastic limit depends on joint velocity," *Journal of Biomechanics*, vol. 44, no. 11, pp. 2106–2112, 2011.

[74] T. A. Wren, K. Patrick Do, S. A. Rethlefsen, and B. Healy, "Cross-correlation as a method for comparing dynamic electromyography signals during gait," *Journal of Biomechanics*, vol. 39, no. 14, pp. 2714–2718, 2006.

[75] M. M. Mukaka, "Statistics Corner : A guide to appropriate use of Correlation coefficient in medical research," vol. 24, no. September, pp. 69–71, 2012.

[76] F. C. Anderson and M. G. Pandy, "Individual muscle contributions to support in normal walking," *Gait and Posture*, vol. 17, no. 2, pp. 159–169, 2003.

[77] S. Kolk, E. M. Klawer, J. Schepers, V. Weerdesteyn, E. P. Visser, and N. Verdonschot, "Muscle Activity during Walking Measured Using 3D MRI Segmentations and [18F]-Fluorodeoxyglucose in Combination with Positron Emission Tomography," *Medicine and Science in Sports and Exercise*, vol. 47, no. 9, pp. 1896–1905, 2015.

[78] A. R. Den Otter, A. C. Geurts, T. Mulder, and J. Duysens, "Speed related changes in muscle activity from normal to very slow walking speeds," *Gait and Posture*, vol. 19, no. 3, pp. 270–278, 2004.

[79] L. Righetti, A. Nylén, K. Rosander, and A. J. Ijspeert, "Kinematic and gait similarities between crawling human infants and other quadruped mammals," *Frontiers in Neurology*, vol. 6, no. FEB, pp. 1–11, 2015.

[80] R. W. Grange, T. G. Gainer, K. M. Marschner, R. J. Talmadge, and J. T. Stull, "Fast-twitch skeletal muscles of dystrophic mouse pups are resistant to injury from acute mechanical stress," *American Journal of Physiology-Cell Physiology*, vol. 283, no. 4, pp. C1090–C1101, 2013.

[81] L. Kiriaev, S. Kueh, J. W. Morley, P. J. Houweling, S. Chan, K. N. North, and S. I. Head, "Dystrophin-negative slow-twitch soleus muscles are not susceptible to eccentric contraction induced injury over the lifespan of the mdx mouse," *American Journal of Physiology-Cell Physiology*, vol. 321, no. 4, pp. C704–C720, 2021.

[82] J. Talbot and L. Mavez, "Skeletal muscle fiber type: using insights from muscle developmental biology to dissect targets for susceptibility and resistance to muscle disease," *Wiley Interdisciplinary Reviews: Developmental Biology*, vol. 5, no. 4, pp. 518–534, 2016.

[83] B. J. Schoenfeld, A. D. Vigotsky, J. Grgic, C. Haun, B. Contreras, K. Delcastillo, A. Francis, G. Cote, and A. Alto, "Do the anatomical and physiological properties of a muscle determine its adaptive response to different loading protocols?," *Physiological Reports*, vol. 8, no. 9, pp. 1–10, 2020.

[84] M. H. Schwartz and A. Rozumalski, "A new method for estimating joint parameters from motion data," *Journal of Biomechanics*, vol. 38, no. 1, pp. 107–116, 2005.

[85] A. Leardini, A. Cappozzo, F. Catani, S. Toksvig-Larsen, A. Petitto, V. Sforza, G. Cassanelli, and S. Giannini, "Validation of a functional method for the estimation of hip joint centre location," *Journal of Biomechanics*, vol. 32, no. 1, pp. 99–103, 1999.

[86] D. G. Thelen, "Adjustment of Muscle Mechanics Model Parameters to Simulate Dynamic Contractions in Older Adults," *Journal of Biomechanical Engineering*, vol. 125, no. 1, pp. 70–77, 2003.

[87] D. D. Shin, J. A. Hodgson, V. R. Edgerton, and S. Sinha, "In vivo intramuscular fascicle-aponeuroses dynamics of the human medial gastrocnemius during plantarflexion and dorsiflexion of the foot," *Journal of Applied Physiology*, vol. 107, no. 4, pp. 1276–1284, 2009.

[88] M. T. Hooijmans, E. H. Niks, J. Burakiewicz, C. Anastasopoulos, S. I. van den Berg, E. van Zwet, A. G. Webb, J. J. Verschuuren, and H. E. Kan, "Non-uniform muscle fat replacement along the proximodistal axis in Duchenne muscular dystrophy," *Neuromuscular Disorders*, vol. 27, no. 1, pp. 458–464, 2017.

Appendix A: Inverse kinematics and inverse dynamics versus reference literature

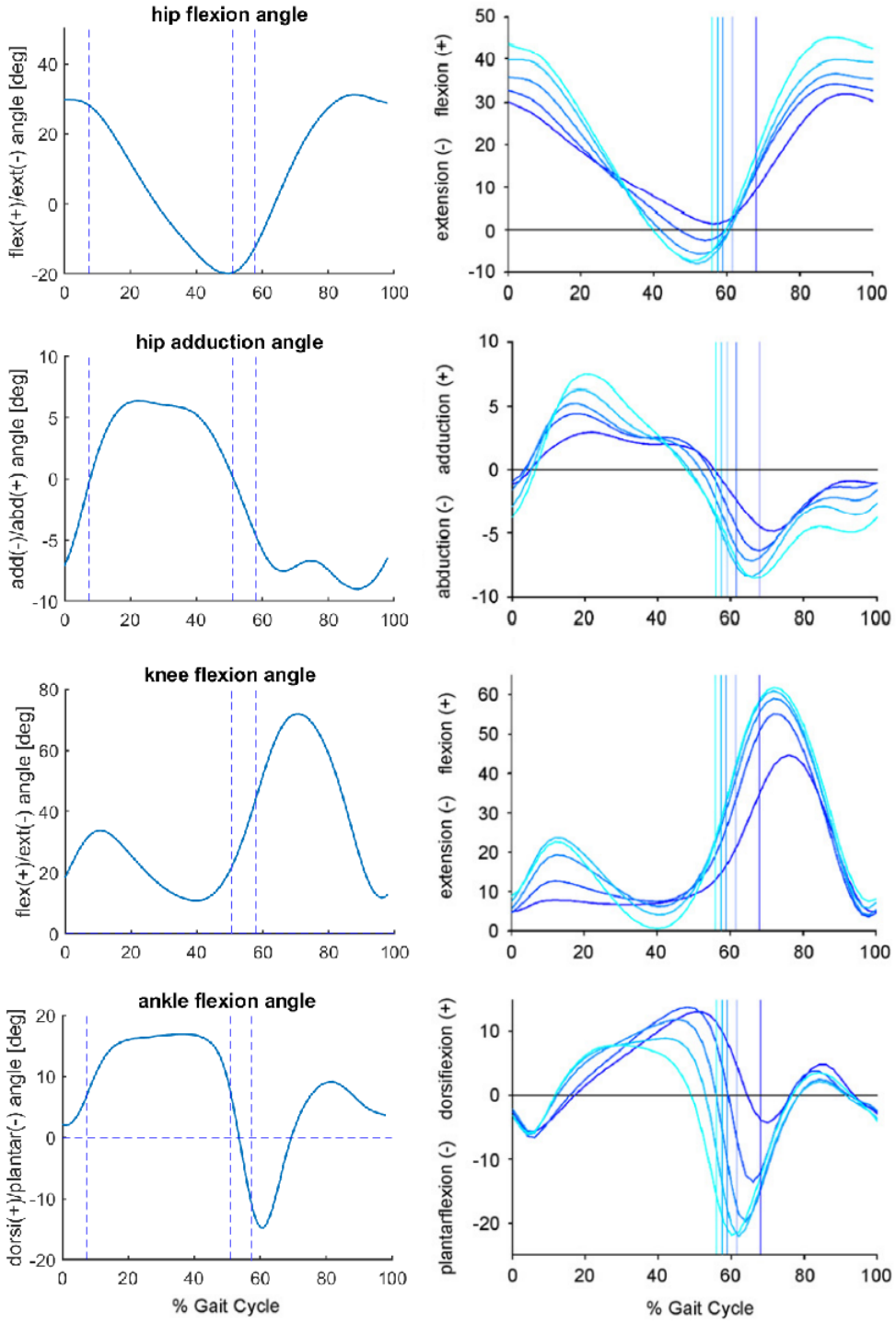

Figure 25: Mean joint angles of subjects analyzed in this study (left) versus reference literature (right) [61].

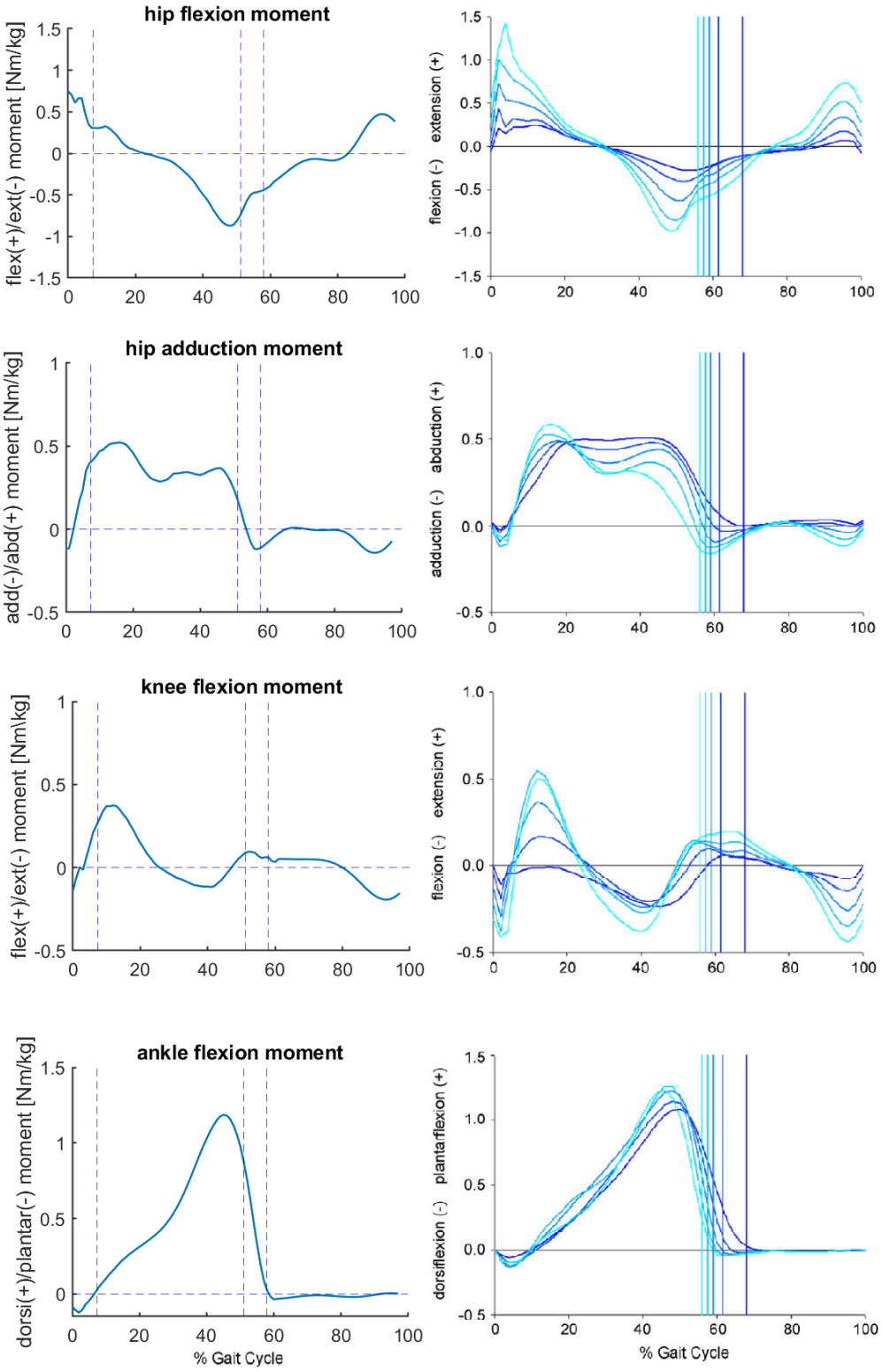

Figure 26: Mean joint angular moments of subjects analyzed in this study (left) versus reference literature (right) [61].

Appendix B: Work values

Normalized negative work: effect of constraining muscles

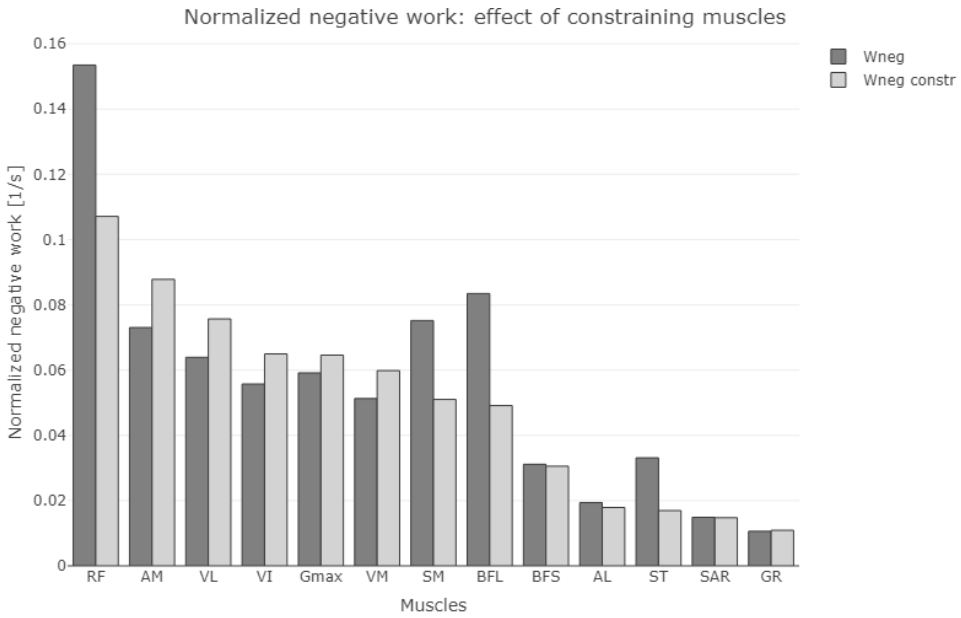

Figure 27: Effect of constraining upper leg muscles on normalized negative work.

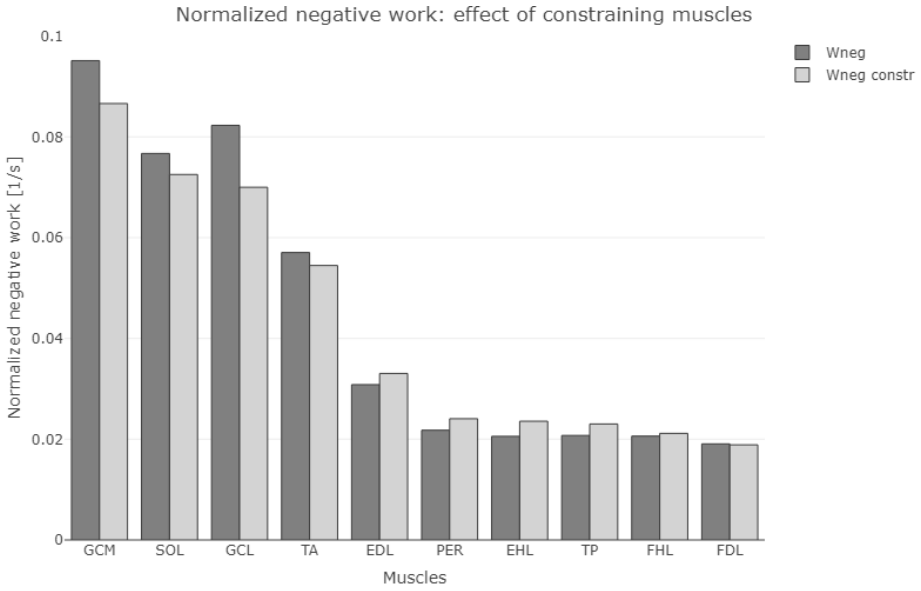

Figure 28: Effect of constraining lower leg muscles on normalized negative work.

Normalized positive work: effect of constraining muscles

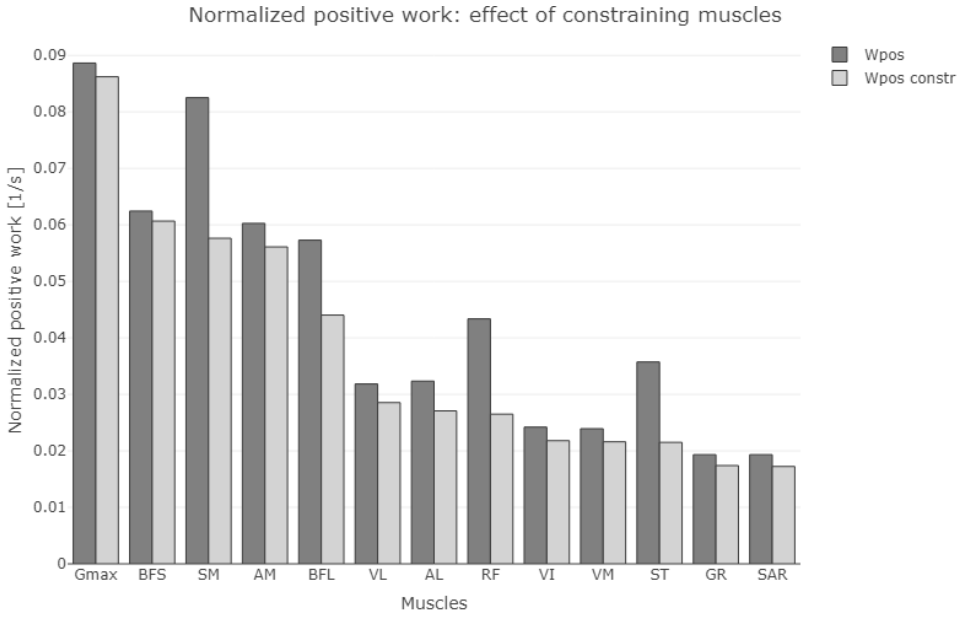

Figure 29: Effect of constraining upper leg muscles on normalized positive work.

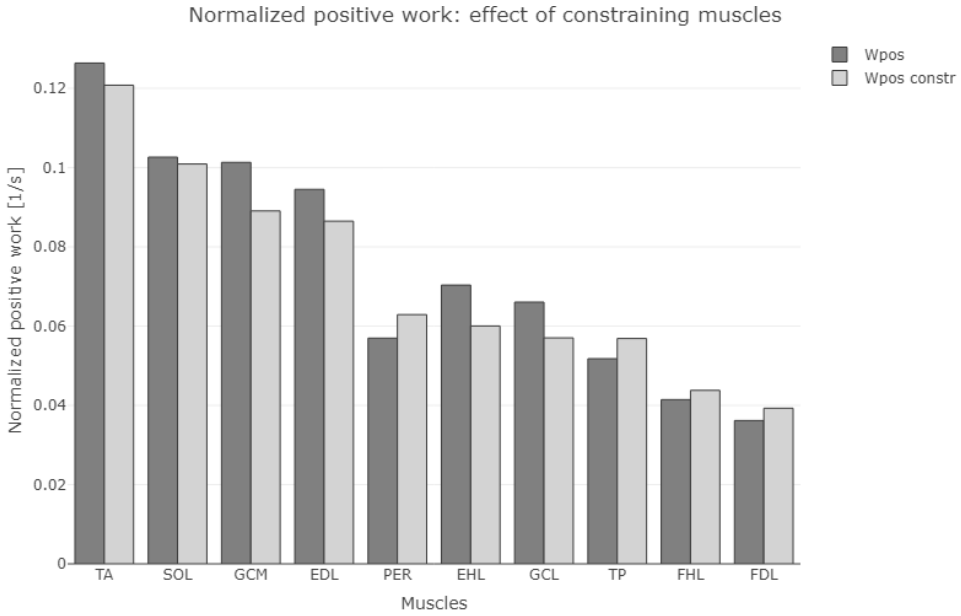

Figure 30: Effect of constraining lower leg muscles on normalized positive work

Total work

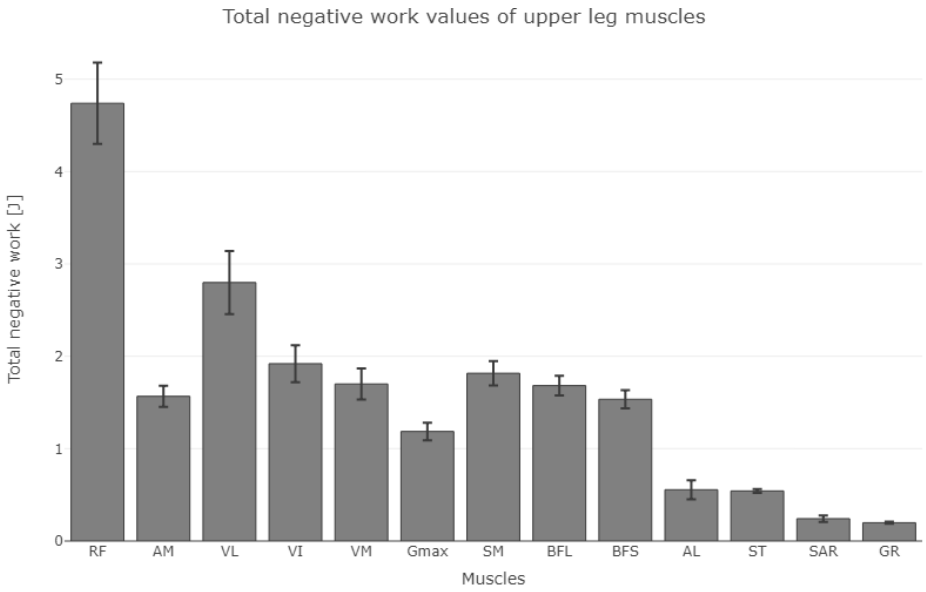

Figure 31: Total negative work values for upper leg muscles.

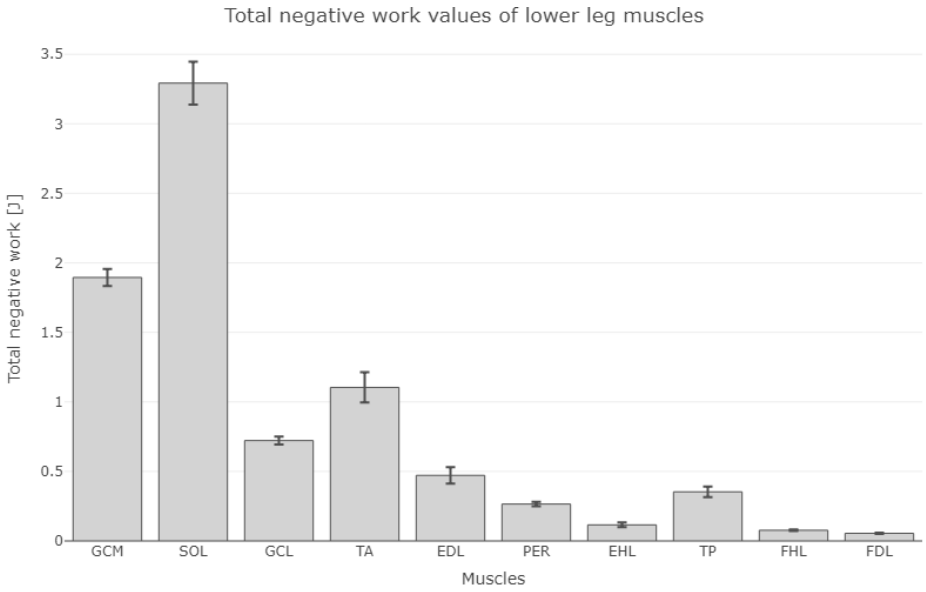

Figure 32: Total negative work values for lower leg muscles.

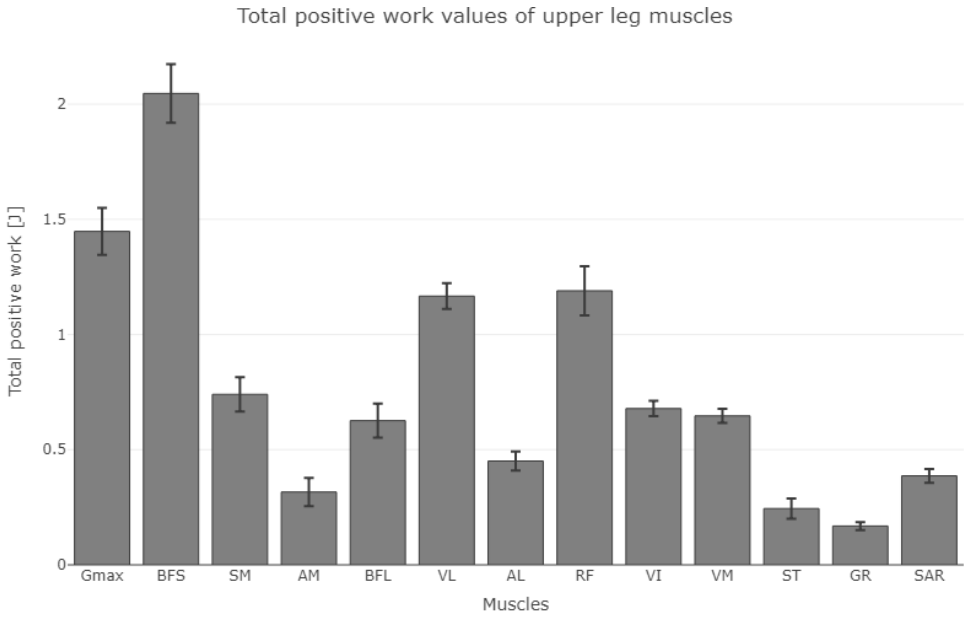

Figure 33: Total positive work values for upper leg muscles.

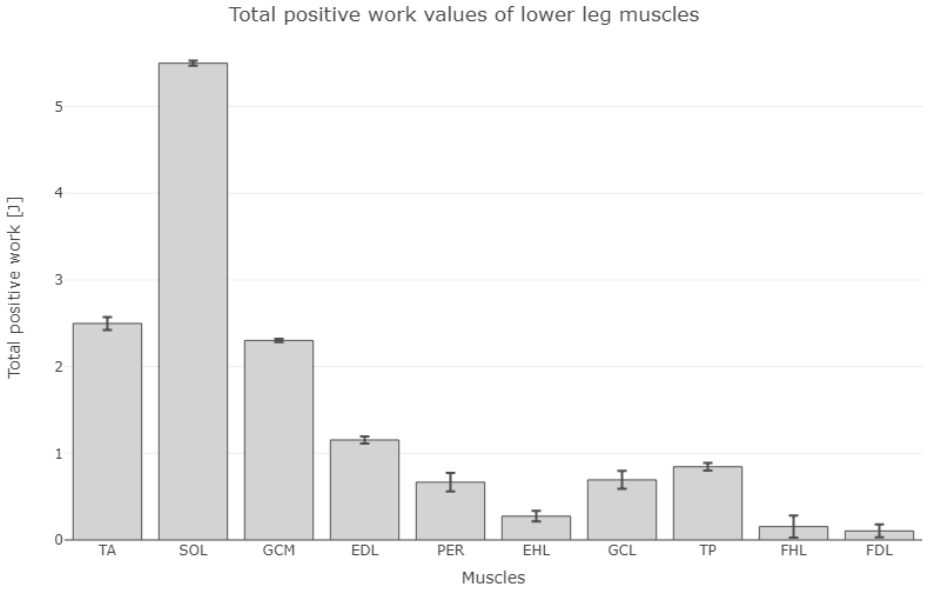

Figure 34: Total positive work values for lower leg muscles.

Appendix C: Absolute work versus muscle fat replacement

Figure 35 shows correlations between normalized absolute work (positive work + negative work) for upper and lower leg muscles separately. A strong correlation was observed for upper leg muscles ($R^2 = 0.85$, $p < .001 * **$). Since both normalized negative and positive work showed significant correlations with fat fractions, this was expected. A moderately strong, yet insignificant correlation was observed for lower leg muscles ($R^2 = 0.33$, $p = .08$), which is weaker than the correlation between normalized negative work and fat fractions.

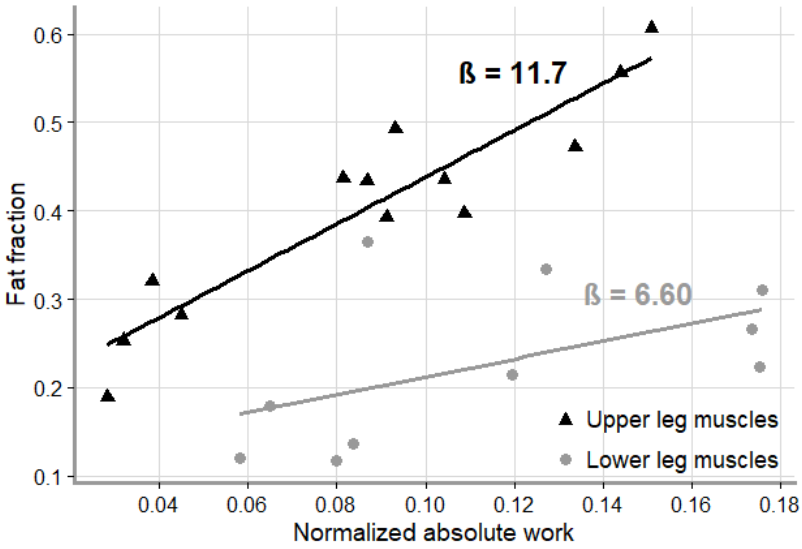

Figure 35: Linear regression between normalized absolute work and fat fraction values for upper and lower leg muscles separately. Slopes of the linear regression line are indicated with β.

An association between normalized absolute work and $logFF$ was observed, as was expected. The association with $logFF$ is not stronger for normalized absolute work than for normalized negative work. The effect of normalized absolute work on $logFF$ is shown in Figure 36.

Table 7: Output multiple-regression model of normalized absolute work versus $logFF$: upper leg muscles versus lower leg muscles.

	Estimate (β)	SE β	95% CI	p-value
$W_{abs,norm}$	6.60	2.45	1.80 - 11.40	.014*
$Part$	1.12	0.15	0.83 - 1.41	<.001*
$W_{abs,norm} \cdot Part$	5.07	3.41	-1.61 - 11.75	.15

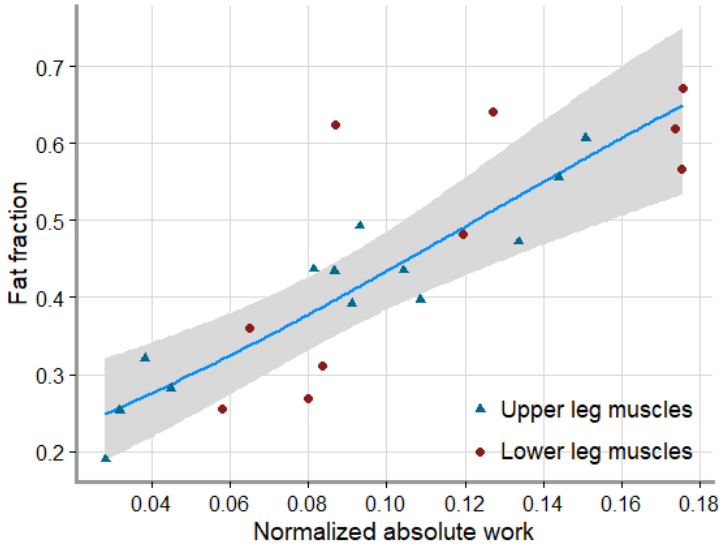

Figure 36: Normalized absolute work was significantly associated with $logFF$ when upper and lower leg muscles are not separated. $logFF$ was transformed back to fat fraction values in the graph.

Individual effects of normalized positive and negative work, as well as their interaction, were also computed in the following multiple-regression model:

$$logFF = \beta_0 \ + \ \beta_1 \cdot W_{neg,norm} \ + \ \beta_2 \cdot W_{pos,norm} \ + \ \beta_3 \cdot W_{neg,norm} \cdot W_{pos,norm}$$

The results are shown in Table 8 below. As can be observed, normalized positive work does not significantly contribute in the association between normalized absolute work and muscle fat replacement.

Table 8: Output multiple-regression model of normalized work versus $logFF$: positive versus negative work.

	Estimate (β)	SE β	95% CI	p-value
$W_{neg,norm}$	17.0	4.60	7.98 - 26.0	.0015*
$W_{pos,norm}$	-5.76	4.34	-14.3 - 2.75	.20
$W_{neg,norm} \cdot W_{pos,norm}$	5.33	176	-341 - 351	.98

Appendix D: gait analysis DMD

The work values from Figures 37-40 resulted from analyzing four gait cycles of one DMD patient. The results are generally agreeable, apart from some obvious differences in work values. More subjects should be analyzed to draw conclusions regarding these differences. Interestingly, in contrast to the results presented in this report, the correlation between normalized negative work and fat fractions of lower leg muscles was significant ($R^2 = 0.41$, $p = .045$). No further differences in statistical significance were found using these work values.

Normalized negative work: unimpaired vs DMD

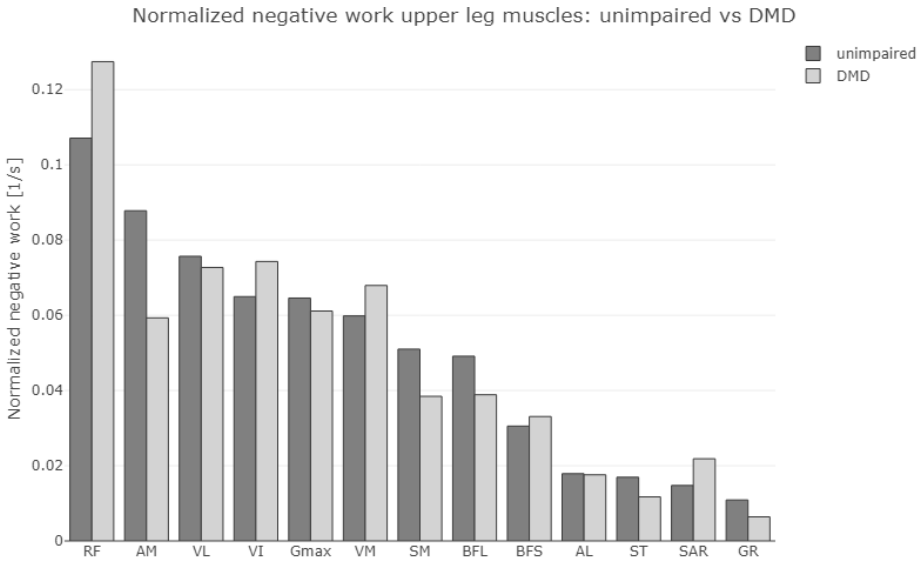

Figure 37: Normalized negative work values of upper leg muscles of one DMD patient compared to the values obtained from unimpaired subjects.

Figure 38: Normalized negative work values of lower leg muscles of one DMD patient compared to the values obtained from unimpaired subjects.

Normalized positive work: unimpaired vs DMD

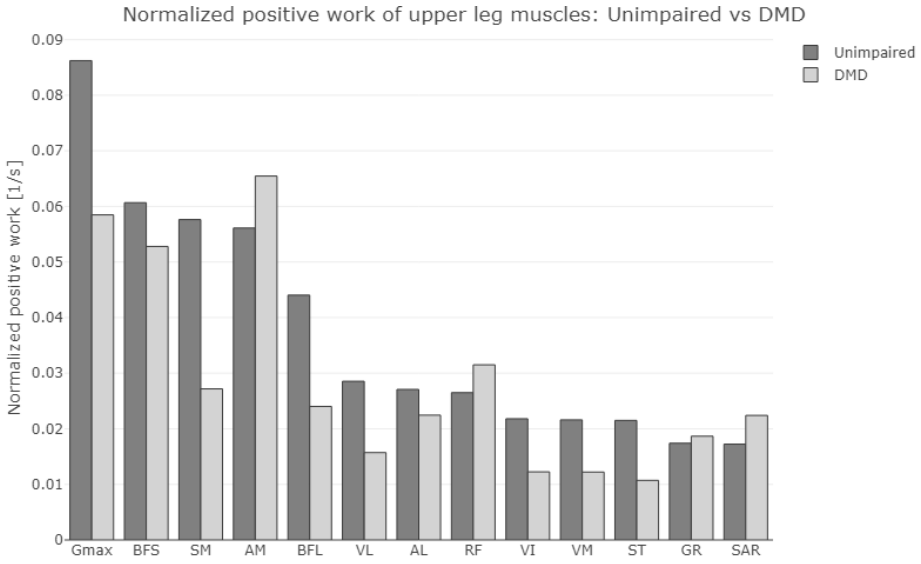

Figure 39: Normalized positive work values of upper leg muscles of one DMD patient compared to the values obtained from unimpaired subjects.

Figure 40: Normalized positive work values of lower leg muscles of one DMD patient compared to the values obtained from unimpaired subjects.